Dust impact on marine biota and atmospheric CO$_2$ during glacial periods

Laurent Bopp,[1] Karen E. Kohfeld, and Corinne Le Quéré
Max-Planck Institut für Biogeochemie, Jena, Germany

Olivier Aumont
Laboratoire d'Océanographie et de Dynamique du Climat, Université Paris VI, Paris, France

[1] We assess the impact of high dust deposition rates on marine biota and atmospheric CO$_2$ using a state-of-the-art ocean biogeochemistry model and observations. Our model includes an explicit representation of two groups of phytoplankton and colimitation by iron, silicate, and phosphate. When high dust deposition rates from the Last Glacial Maximum (LGM) are used as input, our model shows an increase in the relative abundance of diatoms in today's iron-limited regions, causing a global increase in export production by 6% and an atmospheric CO$_2$ drawdown of 15 ppm. When the combined effects of changes in dust, temperature, ice cover, and circulation are included, the model reproduces roughly our reconstruction of regional changes in export production during the LGM based on several paleoceanographic indicators. In particular, the model reproduces the latitudinal dipole in the Southern Ocean, driven in our simulations by the conjunction of dust, sea ice, and circulation changes. In the North Pacific the limited open ocean data suggest that we correctly simulate the east-west gradient in the open ocean, but more data are needed to confirm this result. From our model-data comparison and from the timing of the dust record at Vostok, we argue that our model estimate of the role of dust is realistic and that the maximum impact of high dust deposition on atmospheric CO$_2$ must be <30 ppm. *INDEX TERMS:* 1615 Global Change: Biogeochemical processes (4805); 4255 Oceanography: General: Numerical modeling; 4267 Oceanography: General: Paleoceanography; *KEYWORDS:* Last Glacial Maximum, pCO$_2$, ocean, biogeochemistry, dust, iron

1. Introduction

[2] Air bubbles trapped in Antarctic ice reveal that atmospheric PCO$_2$ during peak glacial times, such as the Last Glacial Maximum, was roughly 80–100 ppm lower than the interglacial times value of 280 ppm [*Barnola et al.*, 1987]. Moreover, they show a tight correlation between atmospheric PCO$_2$ and temperature during the last four glacial/interglacial cycles [*Petit et al.*, 1999]. At the same time, model calculations suggest that PCO$_2$ variations play a significant role in the energetics of glacial/interglacial climate changes by amplifying the glaciations [*Weaver et al.*, 1998]. However, despite the clear importance of atmospheric PCO$_2$ variations for the glacial cycles, we have not yet identified the cause of these variations and this question has persisted for the last two decades.

[3] The turnover time of lithospheric carbon is too slow to account for PCO$_2$ changes over the glacial cycles and it has been shown that the terrestrial biosphere released carbon during glacial periods (the wrong direction to account for lower glacial PCO$_2$) [*Shackleton*, 1977]. Therefore the only remaining candidate to explain atmospheric CO$_2$ glacial-interglacial changes is the ocean.

[4] One family of hypotheses to explain reduced atmospheric CO$_2$ during glacial times relies on physical mechanisms. The solubility of CO$_2$ is increased at low temperature. However, the magnitude of the glacial cooling can account for only a small fraction of the observed PCO$_2$ drawdown [*Sigman and Boyle*, 2000; *Archer et al.*, 2000b]. Moreover, higher salinities during glacial times, through reducing CO$_2$ solubility, would partly cancel out the temperature effect. *Stephens and Keeling* [2000] have proposed that extended winter sea ice prevented outgassing of CO$_2$-rich water around Antarctica during glacial times, but this mechanism requires much less vertical mixing at low latitudes than is normally assumed [*Archer et al.*, 2000a].

[5] Another family of hypotheses invokes biogeochemical processes, through changes of the CaCO$_3$ cycle and changes in marine productivity. Either an increase in the ocean inventory of major nutrients (PO$_4^{3-}$ and NO$_3^-$) [*Broecker*, 1982], or an increased utilization of surface nutrients by marine ecosystems [*Knox and McElroy*, 1984; *Sarmiento and Toggweiler*, 1984; *Siegenthaler and Wenk*, 1984] could have stimulated the oceanic biological pump and thus reduced atmospheric PCO$_2$ during glacial times.

---

[1]Now at Laboratoire des Sciences du Climat et de l'Environnement, Gif sur Yvette, France.

The observations that iron availability limits phytoplankton growth in the ocean [*Martin and Fitzwater*, 1988; *Coale et al.*, 1996; *Boyd et al.*, 2000] and that the supply of iron-rich dust was increased during glacial periods [e.g., *Rea*, 1994; *Petit et al.*, 1999] provide an indirect mechanism by which dust and glacial-interglacial cycles of atmospheric PCO$_2$ are coupled: marine biota could potentially lower atmospheric PCO$_2$ in a dusty and iron-rich glacial climate [*Martin*, 1990].

[6] Here we test this idea of the impact of iron fertilization on ocean primary and export production. A similar study by *Watson et al.* [2000] used a multibox model to test the impact of iron fertilization on the Southern Ocean over multiple glacial-interglacial cycles. Their results showed a drawdown of atmospheric CO$_2$ by 40 ppm. On the other hand, *Archer et al.* [2000b], using an ocean general circulation model with a more primitive biogeochemical cycle, showed that the impact of iron fertilization resulted only in an 8 ppm drawdown of atmospheric CO$_2$. Here we use a state-of-the-art ocean biogeochemistry model, which includes an explicit representation of two groups of phytoplankton and colimitation by iron, silicate and phosphate [*Aumont et al.*, 2003]. This biogeochemical model was embedded in an ocean general circulation model (OGCM), and alternatively forced by glacial and interglacial fields of atmospheric dust deposition [*Mahowald et al.*, 1999], sea-surface temperatures [*CLIMAP*, 1981], sea-ice cover [*Crosta et al.*, 1998a] and ocean circulation (L. Fleury and O. Marti, personal communication, 2002). Glacial-interglacial changes in marine productivity and in atmospheric PCO$_2$ are simulated. In order to evaluate the reliability of our results, we compare our simulated glacial-interglacial changes in export production with observed glacial-interglacial changes using a global compilation of paleoceanographic indicators of export production archived in marine sediments.

2. Method

2.1. Ocean Biogeochemistry Model

[7] We use the Pelagic Interactions Scheme for Carbon and Ecosystem Studies (PISCES) ocean biogeochemistry model. PISCES is based on the Hamburg Ocean Carbon Cycle 5 (HAMOCC5) model [*Aumont et al.*, 2003]. It includes 3 nutrients, 2 phytoplanktons, 2 zooplanktons, one detritus and semilabile dissolved organic matter. It explicitly represents the colimitation of phytoplankton growth by light and three distinct nutrients: phosphate, iron and silicate (see Appendix A for Fe parameterization).

[8] The phytoplankton reservoir is split in two size fractions corresponding to nanophytoplankton and diatoms. Diatoms have two particularities: they require silicate to build their shells and have a lower affinity than nanophytoplankton for nutrients because of their relatively low surface to volume ratio. This lower affinity is modeled by higher half-saturation constants for diatoms compared to nanophytoplankton (Fe limitation, 0.12 nmol L^{-1} versus 0.02 nmol L^{-1}, and PO$_4^{3-}$ limitation, 0.1 μmol L^{-1} versus 0.03 μmol L^{-1}). Consequently, diatoms are favored in regions where Fe or/and PO$_4^{3-}$ are high. Two sizes of zooplankton (microplankton and mesozooplankton) are also
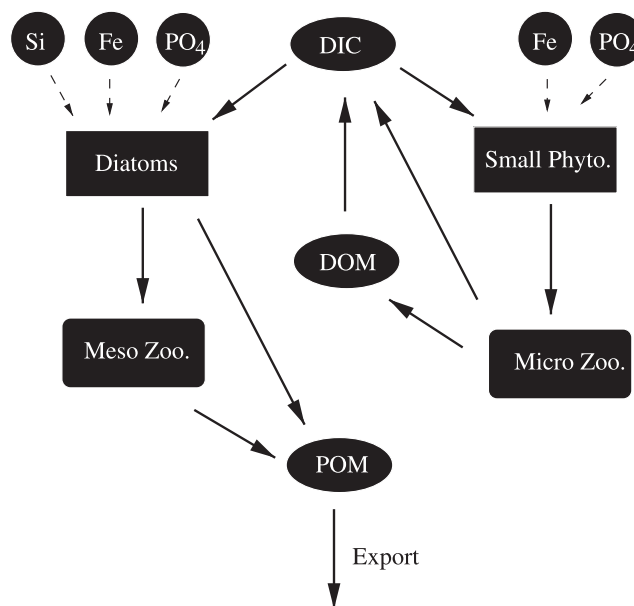

Figure 1. Main compartments of the PISCES ocean biogeochemistry model highlighting the competition between the export production by diatoms and mesozooplankton and the regenerated production by small phytoplankton and microzooplankton.

explicitly considered. This ecosystem representation enables us to distinguish between a "large cells" loop (diatoms and mesozooplankton) which exports carbon efficiently in the intermediate and deep ocean (thus contributes to the export production (EP)), and a "small cells" loop (nanophytoplankton and microzooplankton) which mostly leads to regeneration of the primary production in the euphotic layer (Figure 1).

[9] As a majority of CaCO$_3$ is produced in the ocean by coccolithophorid phytoplankton, a component of the nanophytoplankton, this ecosystem representation also enables us to explicitly represent biogenic siliceous and carbonaceous production through the diatoms/nondiatoms distinction. The model also considers carbonate chemistry and air-sea gas exchange of CO$_2$.

[10] Our model does not include any sediment module or any ocean-sediment interaction, and thus does not consider seafloor CaCO$_3$ burial/dissolution. As a result, these simulations lack all processes implying an input/output budget for alkalinity. Thus a fraction of the LGM-to-present CO$_2$ response would be missing [*Archer and Maier-Reimer*, 1994].

[11] The PISCES model is embedded in an off-line tracer-transport version of the Ocean Parallelisé (OPA) circulation model [*Madec et al.*, 1997]. Resolution averages 4° longitude by 3° latitude with higher meridional resolution at the equator (up to 1°). The vertical grid has 30 levels, 10 of which are in the first 100 m. The deepest layer is 500 m thick and reaches 5000 m depth. Effects of nonresolved sub grid-scale movements are parameterized by horizontal and vertical diffusion. The horizontal diffusivity coefficient is constant everywhere at 2000 m^{-2} s^{-1} and the vertical

diffusivity coefficient is computed prognostically throughout the water column, which allows the mixed layer depth to vary in time and space [*Blanke and Delecluse*, 1993].

2.2. Forcing

2.2.1. Physics/Thermodynamic

[12] To force the tracer-transport model, we use monthly mean fields of temperature, sea ice, oceanic circulation and turbulence, both for present and Last Glacial Maximum states. We use the circulation and turbulence fields computed using the OPA model (L. Fleury and O. Marti, personal communication, 2002) for the present and LGM. The control dynamical simulation (for present time) was forced by climatological winds and fluxes [*Hellermann and Rosenstein*, 1983; *Esbensen and Kushnir*, 1981] and restored to observed sea-surface temperatures and salinities. For the LGM dynamical simulation, the forcing fields of winds and fluxes were perturbed according to an LGM atmospheric simulation [*Pinot et al.*, 1999], and the SSTs, sea-ice fields and SSSs were modified according to LGM reconstructions (respectively, *CLIMAP* [1981] for the SSTs and sea ice, *Duplessy et al.* [1991] for the SSSs). In the LGM simulation, less deep water is formed in the North Atlantic (12 Sv against 18 Sv in the control run) and the deep convection zones are displaced toward the south. In the Southern Ocean, deep convection zones are displaced toward lower latitudes and vertical stratification highly increases south of today's polar front ($\sim$55°S) because of the large increase in LGM sea-ice cover [*CLIMAP*, 1981].

[13] In addition to the dynamical fields described above, we also use for the biogeochemical simulations the SST estimations of Climate: Long-Range Investigation, Mapping, and Prediction (CLIMAP) Project Members (1981), based on the abundance in the sediment of certain species of planktonic microfossils. CLIMAP reconstructions indicate a global mean cooling of 4°C for the glacial sea-surface ocean, which would impact both marine productivity and CO$_2$ solubility. Because the magnitude of LGM tropical cooling is still subject to controversy [e.g., *Sonzogni et al.*, 1998; *Mix et al.*, 1999], we also use an alternative field in which LGM tropical SSTs are cooled by an additional 4°C compared to CLIMAP reconstructions. This additional LGM SST field, the same as used by *Archer et al.* [2000b], will enable us to evaluate the sensitivity of our model's response to the tropical SST cooling uncertainty.

[14] For the biogeochemical simulations, we also impose a sea-ice reconstruction for the LGM around Antarctica based on fossil plankton assemblages [*Crosta et al.*, 1998a, 1998b]. This reconstruction suggests that wintertime Antarctic sea ice extended to the modern Antarctic Polar Front at the LGM, especially in the Atlantic and Indian sector of the Southern Ocean. In summertime, Antarctic sea ice at the LGM may not have been much more extensive than today.

2.2.2. Dust

[15] Stratigraphic records from ice caps [e.g., *Petit et al.*, 1999; *Thompson*, 2000], marine sediments [e.g., *Koopmann*, 1981; *Ruddiman*, 1997], and loess deposits [e.g., *Kohfeld and Harrison*, 2003] show that the dust content of the atmosphere was massively increased during glacial periods. *Mahowald et al.* [1999] have simulated those glacial-interglacial changes using linked terrestrial bio-

sphere, dust source, and atmospheric transport models. They obtain a 2.5-fold higher dust loading in the entire atmosphere in LGM relative to present. The modeled LGM dustiness depends on the expansion of unvegetated areas caused by a combination of increased aridity and low atmospheric CO$_2$. In their simulation, dust deposition increases by a factor of $\sim$2 over the ocean and $\sim$15 in the Southern Ocean.

[16] Data validation suggests that this simulation matches data fairly well, e.g., off NW Africa and in the NW Pacific regions at the LGM (see discussions and *Mahowald et al.* [1999]; *Claquin et al.* [2003]). However, although few dust accumulation rate data from the Southern Hemisphere are available for validation, the overall dust deposition in the Southern Hemisphere appears to be too high at the LGM. For example, while data suggest that dust deposition reaching the Tasman Sea are 3–8 fold higher at the LGM, the *Mahowald et al.* [1999] simulation suggests an LGM increase of 20 to 200 downwind of Australia.

[17] The simulated monthly dust deposition maps of *Mahowald et al.* [1999] for the present and for the LGM are used to force the biogeochemical model. A constant iron content of dust (3.5%), following *Fung et al.* [2000], and a constant solubility for deposited iron (1%), inside the range estimated by *Jickells and Spokes* [2001], are chosen.

2.3. Simulations

[18] Different biogeochemical simulations were carried out for three hundred years each using simulated monthly dust deposition maps of *Mahowald et al.* [1999] for the present or for the LGM, simulated monthly ocean circulation fields of Fleury and Marti (personal communication) for the present or the LGM, reconstructed SSTs of *CLIMAP* [1981] for the present and the LGM, and reconstructed sea-ice cover of *Crosta et al.* [1998a] for the LGM. Comparisons of these simulations allow us to distinguish the relative influence of each forcing field on marine productivity and atmospheric PCO$_2$.

[19] Because of the relative high computer cost of these simulations, only the simulation incorporating all effects (LGM dust, SST from CLIMAP, sea ice and circulation) was run more than 1000 years, i.e., almost to equilibrium.

2.4. Paleodata

[20] In order to assess the change in export production (EP) from the marine record, we compiled several types of paleodata on 123 cores from the literature (Table 1). Each of these proxies has associated assumptions and problems that can complicate its interpretation as a direct indicator of export production. Our approach is to combine information from multiple proxies wherever available in order to minimize the uncertainties and assumptions associated with just one data type. Given the difficulties of comparing several different proxies, our assessment of changes in export production remains qualitative. We only assess whether the EP increased, decreased or remained the same during the LGM compared to today. In instances where the data do not agree we have used the dominant trend when the majority of proxies agree, and keep it undetermined otherwise.

Table 1. Paleodata Table Indicating Name, Position, Dating, and Indication on LGM Export Compared to Present and Reference[a]

Core	Latitude	Longitude	Depth	Dating	a	b	c	d	e	f	g	h	i	j	Reference
North Atlantic Ocean															
PS2212-3	82.07	15.72	2550	$\delta^{18}O$								−			WOL01
PS2138-1	81.53	30.60	995	$\delta^{18}O$								−			WOL01
SU94-20bK	25.00	−16.00	1445	$\delta^{18}O$						+				+	MAR96;SIC00
SU94-20bK	25.02	−16.65	1445	$\delta^{18}O$						+				+	TER00;SIC00
SU94-11K	21.48	−17.95	1200	$\delta^{18}O$						−				−	TER00
GeoB 5559-2	31.65	−13.19	3178	$\delta^{18}O$		+								+	MOR02
GeoB 4216-1	30.63	−12.40	2324	$\delta^{18}O$						+				+	MOR02
Equatorial Atlantic Ocean															
GeoB2910-1	4.85	−21.05	2700	$\delta^{18}O$		+				+					KAS01
GeoB1008-3	−6.58	10.31	3913	$\delta^{18}O$	+	+	+			+					RUT95;SCH97
GeoB1016-3	−11.77	11.68	3411	$\delta^{18}O$		+	0			+				+	MUE94;SCH97;HIN99
Western Equatorial Atlantic Ocean															
GeoB1515-1	4.24	−43.67	3129	$\delta^{18}O$							−	−			RUH96
GeoB1523-1	3.83	−41.62	3292	$\delta^{18}O$		+					−	−			RUH96;KAS01
South Atlantic Ocean															
GeoB1712-4	−23.26	12.81	998	$\delta^{18}O$						+					KIR99
GeoB1711-4	−23.32	12.38	1967	$^{14}C,\delta^{18}O$						+					KIR99
GeoB1710	−23.43	−11.70	2987	$\delta^{18}O$						+	+			+	SCM97;HIN99
GeoB1214	−24.69	7.24	3210	$\delta^{18}O$							0				SCH97;SCM97
RC15-94	−42.98	−20.85	3762	$\delta^{18}O$	+		0	+							KUM95
V22-108	−43.18	−3.25	4171	$\delta^{18}O$	+		+	+	0	+					KUM95;AND98
PS2082-1/3	−43.22	11.74	4661	$\delta^{18}O$	+	0	+	+							FRA00
PS2498-1	−44.17	−14.23	4610					+							KOS96;FRA00
RC15-93	−46.10	−13.22	2714	$\delta^{18}O,^{14}C$	+		+	+	+						KUM95
PS2499-5	−46.52	−15.33	3175					+/0							KOS96;FRA00
PS1754-1/2	−46.77	7.61	2476	$\delta^{18}O$		+	+	+							FRA00
RC13-254	−48.57	−5.57	3636	$\delta^{18}O,^{14}C$	+		+	+	+	+					KUM95;AND98
PS1756-5/6	−48.73	6.71	3803	$\delta^{18}O,^{230}Th$	+	−	+	+							FRA00
RC13-271	−51.98	4.52	3634	$\delta^{18}O$	+		0	+	0						KUM95
PS1768-8/6	−53.61	4.47	3298	$\delta^{18}O,^{14}C$	+	+	+	+							FRA00
RC13-259	−53.88	−4.93	2677	$\delta^{18}O$	0		−	−	−	−					KUM95
RC11-76	−54.38	−22.13	5229					−							KUM95;AND98
PS1772-8/6	−55.46	1.16	4136	$\delta^{18}O$	−	−	0	−							FRA00
PS1575-1	−62.83	−43.33	3461	LC	−	−									BON98
PS1821-6	−67.05	37.47	4027	LC	−	−									BON98
PS1506-1	−68.72	−5.83	2426	LC	−	−									BON98
PS2038-2	−69.35	6.29	1630	LC	−	−									BON98
PS1648-1	−69.73	−6.52	2529	LC	−	−									BON98
PS1375-3	−72.15	−17.10	1750	LC	−	−									BON98
North Pacific Ocean															
XP98-PC1	51.00	152.00	1107	^{14}C			−							−	SEK03
XP98-PC2	51.40	148.33	1258	^{14}C			−							−	SEK03
XP98-PC4	49.50	146.12	664	LC			−							−	SEK03
GGC-15	48.17	151.347	1980	$^{14}C,\delta^{18}O$						+	+			−	KEI98;TER01
H3571	34.90	125.84	3571	$\delta^{18}O$			+			+	+				KAW00
S2612	32.33	157.85	2612	$\delta^{18}O$			+			+	−				KAW99b
ODP 887B	54.37	−148.45	3647	$^{14}C,\delta^{18}O$			0								MCD99
NH22P	21.52	−106.52	2025	$^{14}C,\delta^{18}O$			−			−					GAN98
NH8P	22.39	−107.08	1018	$^{14}C,\delta^{18}O$			0			−					GAN98
NH15P	22.07	−106.48	420	$^{14}C,\delta^{18}O$			−			−					GAN98
ODP 1020	41.00	−126.43	3038	$\delta^{18}O$										−	HER01
ODP 893	34.29	−120.04	575	$^{14}C,\delta^{18}O$						−				−	HER01
ODP 1012	32.28	−118.38	1772	$\delta^{18}O$										−	HER01
LPAZ 21P	22.99	−109.47	624	$\delta^{18}O$										−	HER01
East Equatorial Pacific Ocean															
GS7202-9	4.83	−89.32	3188	$\delta^{18}O$								−			LOU99
RC11-210	1.82	−140.00	4420				?			?	?				REA91;LOU99
P6	0.87	−86.13	2712	^{14}C						+					PED83
RC13-110	0.10	−95.65	3231	$\delta^{18}O$								+			IKE00;LOU99
Y69-71	0.10	−86.48	2740									−			LOU99
P2	−1.41	−92.98	3510	^{14}C						+					PED83,88,91; LOU99
V19-28	−2.47	−84.48	2670	$\delta^{18}O$							+	−			LYL88;LOU99
ODP 846B	−3.10	−90.82	3307	$\delta^{18}O$								−			LOU99

Table 1. (continued)

Core	Latitude	Longitude	Depth	Dating	a	b	c	d	e	f	g	h	i	j	Reference
V19-29	−3.58	−83.93	3157								+				BOY83;LOU99
Y71-9-101	−6.38	−106.94	3175	$\delta^{18}O$								+			IKE00;LOU99
TT013-048	0.12	−139.74	4315	^{14}C						0/−					STE97
TT013-065	0.11	−139.74	4307	^{14}C						0/−					STE97
TT013-069	0.11	−139.72	4307	^{14}C						0/−					STE97
TT013-076	2.07	−140.15	4414	^{14}C						0/−					STE97
TT013-077	2.06	−140.15	4412	^{14}C						0/−					STE97
TT013-098	2.06	−140.14	4413	^{14}C						0/−					STE97
TT013-104	5.08	−139.64	4416	^{14}C						0/−					STE97
PC72	0.00	−140.00	na	$\delta^{18}O$	0	0									MAR01
ODP 680	−11.07	−78.08	252.5	$\delta^{18}O$						−					WEF90
West Equatorial Pacific Ocean															
SCS90-36	18.00	111.49	2050	$^{14}C,\delta^{18}O$						−	−		−		HUA97
NGC34/C2188	3.80	141.49	2188	$\delta^{18}O$			−			−	−				KAW96
KH92-1-5cBX	3.53	141.86	2282	^{14}C						−	+		−		OKH97
C4402	3.00	135.02	4402	$\delta^{18}O$			+			+	+				KAW98
O3187	1.22	160.57	3187	$\delta^{18}O$			?			?	?				KAW99b
South Pacific Ocean															
NGC100	−25.27	162.00	1299	$\delta^{18}O$						0					KAW02
NGC99	−30.00	162.00	1158	$\delta^{18}O$						−					KAW02
17748-2	−32.75	−72.03	2545	^{14}C		+	+			+	+				KLU01;HEB02
GeoB3302-1	−33.22	−72.09	1498	^{14}C		+	+			+	+				KLU01;HEB02
NGC98	−35.00	162.51	1338	$\delta^{18}O$						−					KAW02
NGC97/LH3166	−35.50	161.00	3116	$\delta^{18}O$			?			?	?				KAW02;KAW99a,b
DSDP 594	−45.52	171.95	1204							+					KOW97
TSP-2MC	−48.13	146.90	2283	$\delta^{18}O,^{14}C$										+	IKE00
TSP-2PC	−48.14	146.88	2321	$\delta^{18}O,^{14}C$						0	−			+	IKE00
TSP-3PC	−48.56	146.41	2897	$\delta^{18}O$										+	IKE00
ANTA91-8	−70.78	172.83	2383	^{230}Th		0/−	0/−	0/−		0					CEC98
NB9802-3GC1	−66.13	−169.50	3232	$\delta^{18}O,^{14}C$			0			0	0				CHA03
NB9802-4GC1	−64.2	−170.08	2688	$\delta^{18}O,^{14}C$			−			0	0				CHA03
NB9802-5GC1	−66.11	−169.74	2940	$\delta^{18}O,^{14}C$		0	−			−	−				CHA03
NB9802-6PC1	−61.88	−169.98	3245	$\delta^{18}O,^{14}C$		−	0			0	−				CHA03
E20-10	−60.22	−127.05	4474	$\delta^{18}O,^{14}C$			0				−				CHA03
E11-2	−56.07	−115.09	3111	$\delta^{18}O,^{14}C$			0				−				CHA03
E33-22	−54.93	−120.00	2744	$\delta^{18}O,^{14}C$			0				−				CHA03
Equatorial Indian Ocean															
74KL	14.32	52.38	3212	$\delta^{18}O$					−						MAR01
MD900963	5.06	73.88	2446	$\delta^{18}O$						+		+			BEA00
GC4	−12.28	52.38	2069				+			+	+				MUE00
GC5	−12.37	52.38	1462				+			+	+				MUE00
South Indian Ocean															
E49-21	−42.20	94.90	3328	na			+				−				BAR98
RC11-120	−43.50	79.90	3193	$\delta^{18}O$			+	+			−				BAR98
MD94-102	−43.50	79.80	3205	na			+	+		+	−				BAR98
E49-19	−43.90	90.10	3069	na			+								BAR98
E45-29	−44.90	106.50	3863	na			+								BAR98
MD88-768	−45.80	82.90	3330	na			0/+				−				BAR98
MD88-770	−46.00	96.50	3290	$\delta^{18}O$			+			+	−				BAR98
MD88-769	−46.10	90.10	3420	$\delta^{18}O$			+	+		+	−				BAR98
MD88-767	−46.70	79.50	2920	na			0/−				−				BAR98
E49-23	−47.10	95.10	3206	na			+				−				BAR98
MD88-771	−49.90	100.10	3310	na			+				−				BAR98
MD88-772	−50.00	104.90	3240	na			+	+		+	−				BAR98
KGL 01	−50.70	68.50	1648	na			−			−	−				BAR98
MD88-773	−52.90	109.90	2460	na			−	+		−	−				BAR98
MD84-551	−55.00	73.27	2230	$\delta^{18}O$			−	−		−	−				PIC92;BAR98
MD84-787	−56.40	145.30	3020	na			−	−		−	−				BAR98
MD88-788	−58.00	144.60	3740	na			−			−	−				BAR98
MD84-540	−60.70	86.40	3964	na			−			−	−				BAR98
KR8830	−61.00	93.20	4300	na			−	−		−					BAR98
KR8814	−61.30	144.40	4200	na			−								BAR98
KR8815	−63.30	141.90	3880	na			−			−					BAR98
KR8824	−63.80	116.40	2600	na			−								BAR98
MD88-791	−64.70	119.50	3150	na			−	+		+					BAR98

[21] Direct sediment fluxes of biogenic components, including organic carbon, biogenic opal, carbonate, and biomarkers, all represent some balance between downward fluxes, lateral fluxes, preservation and dissolution of these components. Thus they are not direct representative of export production.

[22] Indirect proxies such as radiogenic isotopes, biogenic barium, authigenic uranium, and benthic foraminiferal abundances all incorporate different assumptions but can be used as organic carbon flux tracers in sediments. Radiogenic proxies (e.g., ^{231}Pa and ^{10}Be), are scavenged by particles in the water column and therefore are related to biogenic and total particulate fluxes [Kumar et al., 1995]. However, they can be affected by extra particle scavenging near continental margins, and preferential adsorption to certain types of particles may affect their ability to record export production exclusively [Frank et al., 2000]. Accumulation of biogenic barium in marine sediments is positively related to organic carbon fluxes (specifically diatom frustules), as barite forms during the decomposition of planktonic marine organic matter [Paytan et al., 1996]. However, interpretation of barium depends on variable ratios of barium to organic material, preservation problems under reducing ocean water conditions, and regional variability in the lithogenic contribution to barium concentrations [McManus et al., 1998]. Authigenic U is formed in marine sediments during the degradation of organic material, and thus is indirectly related to organic carbon fluxes [Kumar et al., 1995]. However, it can also be influenced by lateral fluxes of organic carbon during sediment focusing, as well as low oxygen content of overlying bottom waters [Frank et al., 2000]. The accumulation rates of benthic foraminifera are also believed to increase in response to high organic matter fluxes [Herguera, 1992, 2000]. However, interpretations can be complicated by lateral influxes of carbon as well as poorly understood physiological responses of benthic populations to temperature and reduced oxygen levels [Jorissen et al., 1992].

[23] In addition to preservation and dissolution processes, the accumulation rate of all of these sedimentary components can be affected by sediment redistribution processes which enhance accumulation rates of materials by as much as sixfold in the equatorial Pacific [Marcantonio et al., 2001b], and 20-fold in the Southern Ocean [Francois et al., 1993]. These problems can be circumvented by normalizing fluxes to a proxy with a known water column production rate and flux, such as ^{230}Th [Bacon, 1984]. This procedure improves the reliability of the export fluxes, and is used in 54 out of 123 sites.

[24] The age control for each site was taken from the literature (indicated in Table 1). For the most part sites depended on marine isotope stratigraphy. 32 sites used radiocarbon control for their age models. Age model correlations based on lithogenic or biostratigraphic information alone were used on 7 sites [Bonn et al., 1998].

3. Modern Marine Biota

[25] A thorough comparison to nutrient and chlorophyll data has been performed to validate the biogeochemical scheme. Aumont et al. [2003] have shown that this biogeochemical scheme is able to correctly simulate the main characteristics of the ocean biogeochemistry. In particular, the model reproduces the paradoxical high nutrient low chlorophyll areas (equatorial Pacific, Southern Ocean, North Pacific), where phytoplankton growth is iron-limited. Furthermore, the model also predicts that phytoplankton growth is limited by phosphate in the oligrophic gyres, and that diatoms are specifically limited by silicate in the North Atlantic and in some parts of the Southern Ocean [Aumont et al., 2003]. According to this biogeochemical model, upwelling and mixing constitute the major source of iron for new production, with aeolian deposition only representing about a fourth of the demand for new iron [Aumont et al., 2003].

[26] In the version used for this study, the simulated annual net primary production for the modern global ocean is 58.9 PgC y^{-1}. This value is consistent with the most recent estimates based on remote sensing (54–59 PgC y^{-1}, [Behrenfeld et al., 2001]). Simulated EP is 13.3 PgC years^{-1} in the control simulation for the modern global ocean. This estimate falls in the range of particulate organic carbon (POC) export production estimated from observations (3.5–20 PgC y^{-1}) [Berger and Wefer, 1991; Jahnke, 1996; Laws et al., 2000; Schlitzer, 2002] as well as that from simulations with other global carbon cycle models (8.5–15 PgC y^{-1}) [e.g., Yamanaka and Tajika, 1996; Six and Maier-Reimer, 1996; Aumont et al., 2002].

[27] Our zonal mean of export production is compared to data-based estimates (Figure 2). Because of the sparseness of direct flux measurements and the large uncertainties associated with nondirect estimates, we have three of those

---

Note to Table 1

[a]The different proxies used here are (see text for details on each proxy): a, ^{10}Be; b, biogenic barite; c, biogenic opal; d, authigenic uranium; e, xs(Pa/Th)$_0$; f, organic carbon flux; g, carbonate; h, benthic foraminifera accumulation; i, coccolithophorids assemblage; and j, other biomarker accumulation. Authors abbreviations in the reference column are: AND98 for Anderson et al. [1998], BAR98 for Bareille et al. [1998], BEA00 for Beaufort [2000], BON98 for Bonn et al. [1998], BOY83 for Boyle [1983], CEC98 for Ceccaroni et al. [1998], CHA03 for Chase et al. [2003], FRA00 for Frank et al. [2000], GAN98 for Ganeshram and Pedersen [1998], HEB02 for Hebbeln et al. [2002], HER01 for Herbert et al. [2001], HIN99 for Hinrichs et al. [1999], HUA97 for Huang et al. [1997], IKE00 for Ikehara et al. [2000], KAS01 for Kasten et al. [2001], KAW96 for Kawahata and Eguchi [1996], KAW98 for Kawahata et al. [1998], KAW99a for Kawahata et al. [1999], KAW99b for Kawahata [1999], KAW00 for Kawahata et al. [2000], KAW02 for Kawahata [2002], KEI98 for Keigwin [1998], KIR99 for Kirst et al. [1999], KLU01 for Klump et al. [2000], KOS96 for Koschmeider [1996], KUM95 for Kumar et al. [1995], LOU99 for Loubere [1999], LYL88 for Lyle et al. [1988], MAR01 for Marcantonio et al. [2001a], MAR96 for Martinez et al. [1996], MCD99 for McDonald et al. [1999], MOR02 for Moreno et al. [2002], MUE00 for Mueller and Opdyke [2000], MUE94 for Mueller et al. [1994], OKH97 for Okhouchi et al. [1997], PED83 for Pedersen [1983], PED88 for Pedersen et al. [1988], PED91 for Pedersen et al. [1991], PIC92 for Pichon et al. [1992], REA91 for Rea et al. [1991], RUH96 for Ruhlemann et al. [1996], RUT95 for Rutsch et al. [1995], SCH97 for Schneider et al. [1997], SCM97 for Schmiedl and Mackensen [1997], SEK03 for Seki et al. (Reconstruction of paleoproductivity in the Sea of Okhotsk over the last 20 kyr, submitted to Paleoceanography, 2003, hereinafter referred to as Seki et al., submitted manuscript, 2003), SIC00 for Sicre et al. [2000], STE97 for Stephens and Kadko [1997], TER00 for Ternois et al. [2000], TER01 for Ternois et al. [2001], WEF90 for Wefer et al. [1990], and WOL01 for Wollenburg et al. [2001].

a)

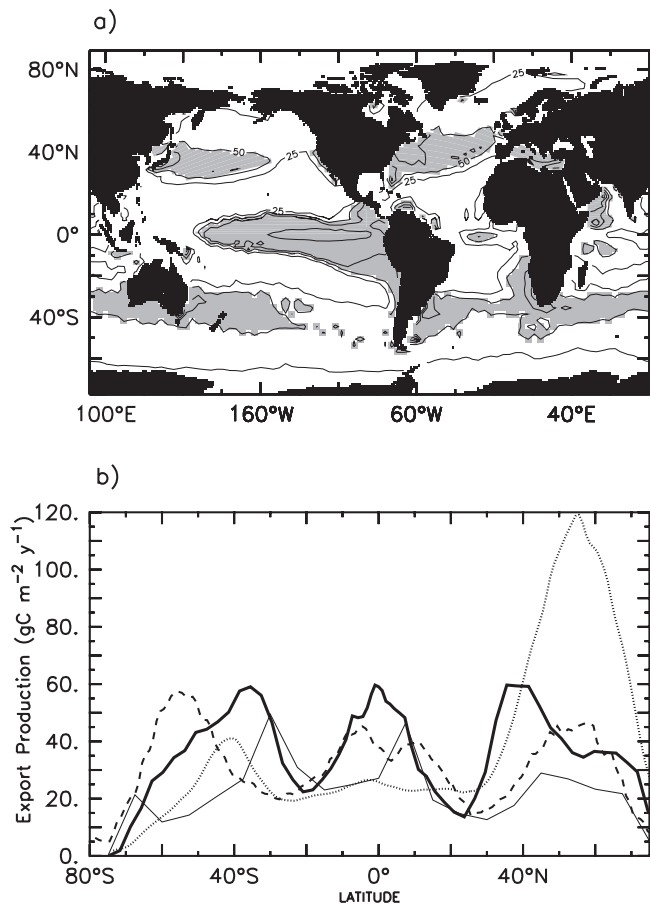b)

Figure 2. (a) Particulate export production (EP) in the control simulation (contours are every 25 gC m^{-2} y^{-1} and shaded areas denote regions where EP > 50 gC m^{-2} y^{-1}). (b) Zonal mean of particulate export production (in gC m^{-2} y^{-1}), simulated by our model (heavy solid line), estimated from inverse modeling [*Schlitzer*, 2002] (dashed line) and satellite-based (from *Laws et al.* [2000] (dotted line) and from the CZCS ocean color archive and the *Berger and Wefer* [1991] algorithm (thin solid line)).

estimates, two based on remote sensing of ocean color and one on inverse modeling of oceanographic data. We first exploit the primary production that was computed from the CZCS ocean color archive [*Antoine et al.*, 1996] and use a simple algorithm [*Berger and Wefer*, 1991] to derive the export production. Second, we use the export production estimates from *Laws et al.* [2000], based on SeaWiFs ocean color archive and a more complex algorithm to derive the export production. Third, we use the export production estimates from *Schlitzer* [2002], based on inverse modeling of oceanographic (hydrographic, oxygen, nutrient, and carbon) data. Given the large uncertainties associated with such derivations and the differences between the data-based estimates, export production simulated by our model is generally consistent with those derived from observations (Figure 2).

[28] Simulated rain ratio (the molar ratio of the downward CaCO₃ flux to the downward POC flux at the base of the euphotic layer) is 0.053 in our control simulation. This number falls below the typical model-specified range of 0.15–0.25 [e.g., *Aumont et al.*, 2002], but our model prediction is consistent with a new estimate of the rain ratio, based on observations of the vertical gradients of alkalinity and nitrate, which indicates a global average of 0.06 ± 0.03 [*Sarmiento et al.*, 2002].

4. Marine Biota at LGM

4.1. Simulated Dust Impact

4.1.1. Shift of Phytoplankton Assemblages

[29] When high dust deposition rates from the LGM are used on modern ocean, surface iron concentration increases everywhere in the ocean and drives a shift in the marine phytoplankton assemblage from nanophytoplankton to diatoms (Figure 3a) in today's iron-limited regions (North Pacific, part of the Southern Ocean, equatorial Pacific). In particular, the contribution of diatoms to the marine phytoplankton assemblage increases by 50% in the North Pacific, by 30% off the Patagonian Plateau and west of Australia. For the zonal mean (Figure 3a), the increase is general with its maximum between 10 and 30% at 40°N–70°N and at 60°S–30°S. The differential response of diatoms and nanophytoplankton to an increase in sea-surface iron concentrations, and the changes of the phytoplankton ecosystem that follows, is explained by the different half-saturation constants that have been chosen for the two groups of phytoplankton.

4.1.2. Production Changes

[30] This shift of species is responsible for major changes in the regional patterns of export production (EP) (Figure 3c) and for its global increase by 0.7 PgC y^{-1} (+6%) (Table 2). Globally, when LGM dust field is used, EP is enhanced from 13.3 PgC y^{-1} to 14.1 PgC y^{-1}. Regionally, EP increases in areas where nanophytoplankton are replaced by diatoms. The increase reaches +30–50 gC m^{-2} y^{-1} in the North Pacific, southwest of Australia and off the Patagonian Plateau. In the equatorial Pacific, EP also increases but this increase is balanced by a reduction of EP north and south of the equatorial tongue. In the same way, EP increase in the Benguela upwelling is counterbalanced by a pronounced diminution westward (−20 gC m^{-2} y^{-1}).

[31] In parallel with the increase of export production with LGM dust deposition, the total primary production (PP) remains more or less constant (from 58.9 PgC y^{-1} for modern dust deposition to 58.7 PgC y^{-1} in case of LGM dust deposition). This decoupling between EP and PP can be explained by the conjunction of two factors, an increase in the export efficiency (e ratio, defined in the model as the fraction of PP that is exported below 120 m) and an increase in the oligotrophic gyres areas.

[32] 1. Export efficiency increases as diatoms export carbon more efficiently than nanophytoplankton (they sink more rapidly and are grazed less efficiently). Consequently, the mean e ratio increases from 0.22 to 0.24 with higher dust deposition and leads to an increased EP.

[33] 2. Oligotrophic areas increase because diatoms export macronutrients more efficiently in the productive regions and thus waters advected toward the oligotrophic
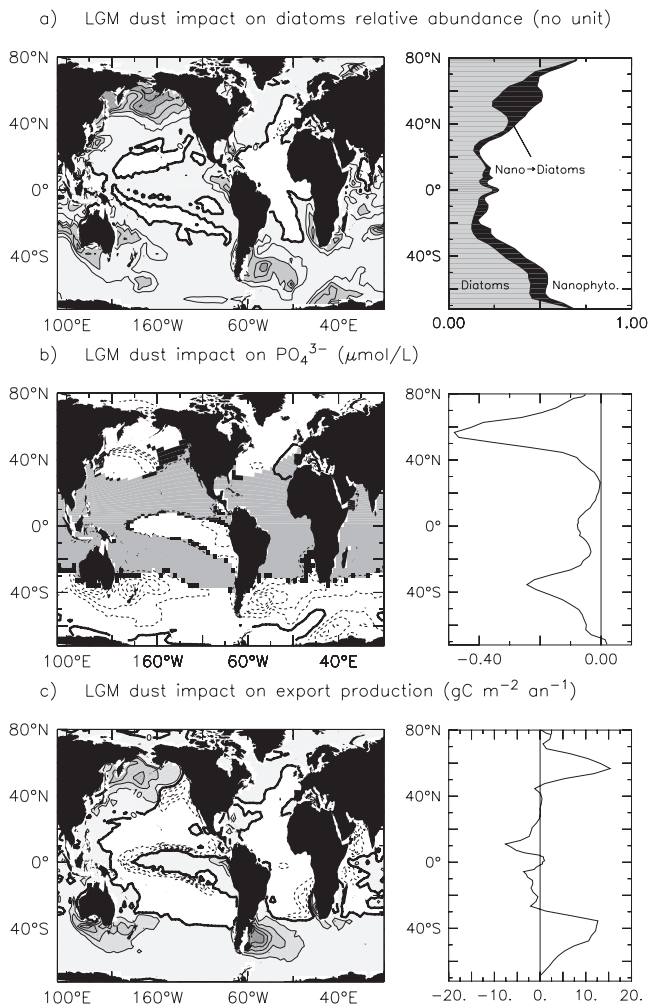
a)   LGM dust impact on diatoms relative abundance (no unit)

b)   LGM dust impact on PO₄³⁻ (μmol/L)

c)   LGM dust impact on export production (gC m⁻² an⁻¹)

Figure 3. Simulated impact of dust deposition during the LGM on changes in (a) the relative abundance of diatoms during the LGM compared to modern marine biota (contours are every 10%, shaded areas denote increased relative abundance of diatoms during the LGM); (b) PO_4^{3-} concentrations in surface waters (contours are every 0.1 μmol l⁻¹, shaded areas denote oligotrophic gyres in the control simulation determined by $PO_4^{3-} < 0.25$ μmol l⁻¹, and black areas denote regions turning to oligotrophic areas with LGM dust deposition); and (c) export production of carbon at 120 m (contours every 10 gC m⁻² y⁻¹, shaded areas denote increased EP during the LGM). On the right of each map is added a zonal mean of the LGM relative to present changes.

Table 2. Increase in Dust Deposition and Its Effects on Modern Ocean Conditions

	Modern Dust	LGM Dust
Dust deposition, 10⁹ mol years⁻¹	265	465 (×1.75)
EP, PgC years⁻¹	13.3	14.1 (+6%)
PP, PgC years⁻¹	58.9	58.7 (−0.3%)
e ratio	0.22	0.24 (+8%)
P.CaCO₃, PgC years⁻¹	0.70	0.68 (−2%)
Rain ratio	0.053	0.048 (−8%)
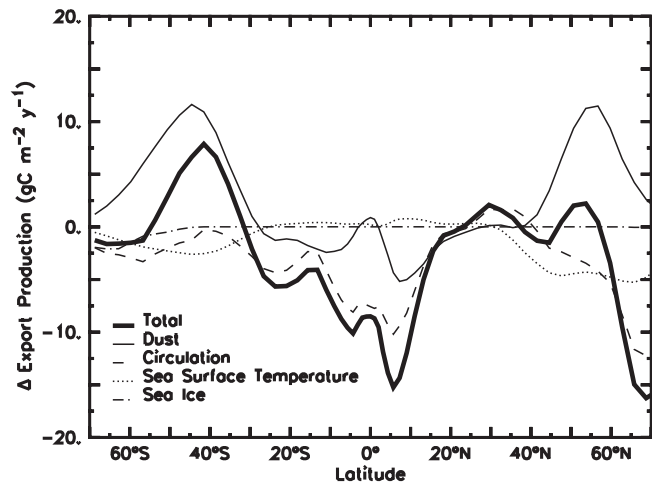
Figure 4. Simulated impact of LGM dust deposition (solid line), LGM circulation (dashed line), LGM SSTs (dotted line), LGM Antarctic sea ice (dot-dashed line) and LGM all-effects (heavy solid line) on export production (zonal annual mean, in gC m⁻² y⁻¹). See text for details.

regions are more depleted in nutrients (Figure 3b). The increase in oligotrophic areas reaches 9%, (from $1.69 \cdot 10^{14}$ to $1.85 \cdot 10^{14}$ m²) and is responsible for the slight decrease in PP.

[34] The increased dust deposition also leads to changes in biogenic silica and biogenic calcite productions. Whereas the export production of siliceous tests is increased (+2%), the export production of calcareous tests slightly diminishes (−3%). In conjunction with increased export of organic particles (POC) (+6%), the decreased biogenic calcite production leads to a decreased rain ratio (the molar ratio of the downward $CaCO_3$ flux to the downward POC flux). At 120 m, the rain ratio is decreased by 8% (from 0.053 to 0.048). Alkalinity distribution and CO_2 fluxes are affected by these changes (see section 5.1).

4.2. Other Effects: Temperature, Sea Ice, and Circulation

[35] To compare our simulated changes in export production to available paleodata, we use a simulation of the LGM which combines the effects of changes in SSTs [*CLIMAP*, 1981] without additional SST cooling in the tropics), sea ice [*Crosta et al.*, 1998a] and ocean circulation (L. Fleury and O. Marti, OPA model) (Figures 4 and 5; Table 3). The LGM-all effects simulation shows significant differences from the LGM-dust only simulation. The mean export production is reduced by 7% whereas it is increased by 6% in the dust-only case (Table 3). Regional patterns of changes in the LGM-all effects simulation are also quite different from the dust-only case: export production strongly decreases in the equatorial Pacific, decreases also south of 50°S in the Southern Ocean and in the North Atlantic (Figure 5).

[36] Additional simulations, taking into account each mechanism individually (SSTs, sea ice and circulation) enable us to analyze each effect separately (Figure 4). The sum of all effects taken separately does not exactly match
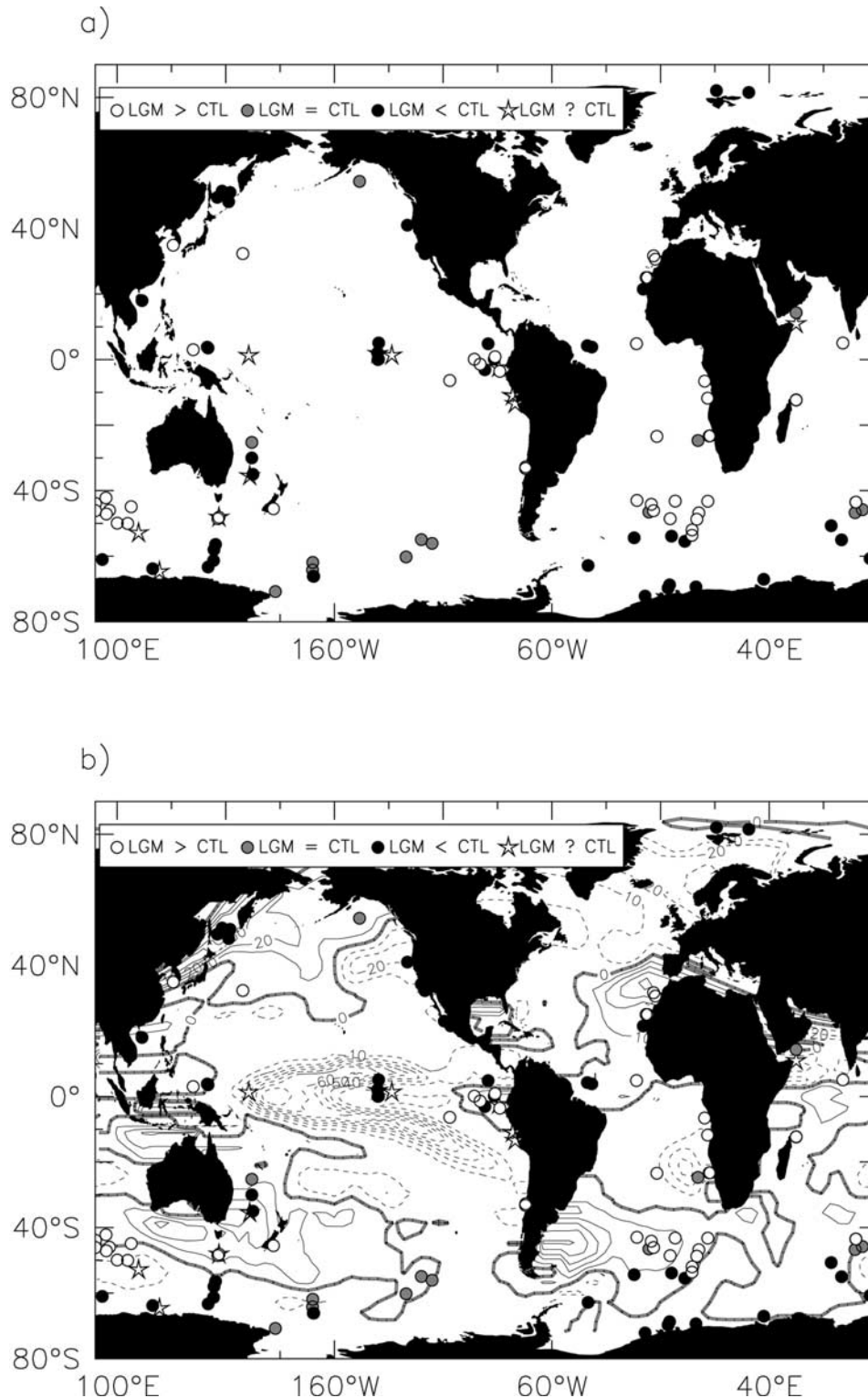
Figure 5. Export production (EP) for the LGM minus today. (a) The top panel shows whether the EP increased (LGM > CTL), decreased (LGM < CTL), remained the same (LGM = CTL) or is undetermined (LGM ? CTL) during the LGM compared to today (CTL for control). This information is based on our analysis of various paleodata indicators (complete references of the data sources is given in Table 1). (b) The bottom panel shows a comparison of simulated changes in export production ($gC/m^2/y$) with the paleoceanographic data. The simulated changes combine effects of LGM dust [*Mahowald et al.*, 1999], Antarctic sea ice [*Crosta et al.*, 1998a], SSTs [*CLIMAP*, 1981], and circulation changes. See color version of this figure at back of this issue.

Table 3. Effect of LGM Conditions on Export Production and Atmospheric PCO$_2$

	EP, PgC Years^{-1}	Percent Changes in EP	PCO$_2$ Changes, ppm
Control	13.3	-	-
Dust	14.1	+6	−15 (+3/−39)[a]
Circulation	12.0	−12	−3
Sea ice	13.25	−1	+1 (+1)[b]
Temperature	13.0	−3	−22 (−28)[c]
Salinity	13.3	−	+6
All effects[d]	12.5	(−7)	−32

[a]The numbers in parenthesis correspond to additional sensitivity tests: the first one uses no iron deposition from the atmosphere, the second one prescribes an iron-saturated surface ocean.

[b]The number in parenthesis corresponds to an additional sensitivity test in which LGM sea-ice cover was set all year-round to its winter value.

[c]The number in parenthesis corresponds to an additional sensitivity test in which LGM tropical SSTs are cooled by an additional 4° compared to CLIMAP reconstructions.

[d]The LGM all-effects simulation includes the combined effects of dust, temperature (without additional SST cooling in the tropics), salinity, ice cover and circulation.

the LGM-all effects case because these processes are not independent (Table 3).

[37] Sea-surface cooling leads to a slight reduction of export production (−3%), located at middle and high latitudes (Figure 4). Increased sea-ice cover in the Southern Ocean also leads to a decrease of export production, but almost negligible (−1%) at a global scale as summertime Antarctic sea ice at LGM is taken to be very similar from today's sea ice [*Crosta et al.*, 1998a].

[38] Circulation changes simulated with the OPA model for the glacial conditions cause significant modifications of export production (Figure 4). The global mean EP is decreased by over 10% and this decrease is almost general (Figure 4). In the Southern Ocean, export production is mainly controlled by iron surface concentrations and our simulation shows a decrease of those concentrations (~−0.1 nM) south of 50°S, following increased vertical stratification and decreased mixing with iron-rich subsurface waters. In the equatorial Pacific, the upwelling intensity is reduced for the LGM and leads to a strong decrease of export production (Figure 4), mainly located on the edges of the equatorial tongue. Those regional changes in EP due to the LGM circulation are obvious in the LGM-all effects simulation (Figure 5).

4.3. Comparison With Observed Changes in Export Production
4.3.1. Southern Ocean
[39] Data from the South Pacific suggest little change or slight decrease in export production [*Chase et al.*, 2003]. However, data from the South Atlantic and Indian Oceans clearly indicate a lower export production south of the modern-day Polar Front, and higher export between approximately 53.5°S and 40°S [*Anderson et al.*, 1998; *Bareille et al.*, 1998; *Bonn et al.*, 1998; *Frank et al.*, 2000; *Kumar et al.*, 1995]. The model reproduces this dipole, which is driven in our model both by changes in dust deposition and circulation. However, the position of this dipole is displaced to the south in the Atlantic basin, to the north in the Indian basin. A

possible cause for the shift in latitude in the Atlantic basin is that the glacial-interglacial change in dust deposition simulated by *Mahowald et al.* [1999] may be too large.
4.3.2. Upwelling Regions
[40] In the upwelling regions of west Africa (6°S to 25°S) [*Schneider et al.*, 1995, 1997; *Kasten et al.*, 2001; *Rutsch et al.*, 1995] and South America (35°S) [*Klump et al.*, 2000; *Hebbeln et al.*, 2002], the data indicate an increase in export which is not reproduced by the model. The model/data discrepancy may be due to the fact that the upwelling regime is not well reproduced there mainly because of the coarse resolution of our model. Furthermore, west Africa is also influenced by increases in fluvial input from the Zaire River which could regionally increase the nutrient and silica supply [*Schneider et al.*, 1995], a process that is not simulated.
4.3.3. Equatorial Pacific
[41] In the equatorial Pacific, assessment of changes in export production from paleodata are more ambiguous, primarily because of sediment redistribution. For example, along 140°E, data that have not been normalized using ^{230}Th suggest higher productivity [*Paytan et al.*, 1996] while ^{230}Th-normalized data, which correct for sediment redistribution, suggest that glacial export production was slightly lower or unchanged compared with today [*Stephens and Kadko*, 1997; *Marcantonio et al.*, 2001a]. The latter data suggest that the sign of the change in the model in the central equatorial Pacific is correct, but the magnitude of the changes cannot be verified. In addition, the model shows large differences between the eastern equatorial Pacific where EP is higher at LGM, and the western and central equatorial Pacific where EP is strongly reduced under LGM conditions. Such differences are again explained by the conjunction of dust and circulation changes: higher LGM dust deposition causes an increase of EP in the eastern part of the basin and also leads to decreased EP elsewhere in the equatorial Pacific because of the decrease of nutrients advected from the upwelling zone toward the edges of the equatorial tongue. Because the intensity of the simulated equatorial upwelling is decreased at the LGM, simulated circulation changes drive a reduction of EP in the western and central part of the basin. This decrease accounts for a large part of the global EP reduction simulated by the model (Table 3). More data (and more data that is regionally consistent, e.g., in the eastern equatorial Pacific) are needed to determine if the simulated processes are realistic.
4.3.4. North Pacific
[42] The model results suggest a strong east-west gradient in EP at the LGM. Some of the N. Pacific data support this pattern: data show glacial increases in EP in the midlatitude NW Pacific [*Kawahata*, 1999; *Kawahata et al.*, 2000], little or no change in the Gulf of Alaska [*McDonald et al.*, 1999]; and decreases in EP on the west coast of North America [*Herbert et al.*, 2001]. The major exception to this pattern is observed in the Sea of Okhotsk [*Ternois et al.*, 2001; *Seki et al.*, 2003; Seki et al., submitted manuscript, 2003], where EP was consistently lower at the LGM compared with today. The authors suggest that decreases in productivity resulted from a more extensive sea ice coverage and surface water stratification. In the model, the east-west dipole is entirely driven by higher dust deposition rates. The little or

no change in the Gulf of Alaska coupled with the Sea of Okhotsk data suggests that this simulated increase in EP at the LGM may be too high, and that some physical processes (such as extended sea ice in the Sea of Okhotsk) is missing from this simulation. Additional EP data from the open ocean North Pacific is required to solidly confirm this result.

4.3.5. North Atlantic

[43] Interpretation of changes in paleoexport production in the North Atlantic region are complicated by a large glacial influx of ice-rafted detrital material [*Manighetti and McCave*, 1995], which could account for more than 80% of the organic carbon accumulating in this region [*Villanueva et al.*, 1997]. Two points from the high Arctic region, based on benthic foraminiferal abundances [*Wollenburg et al.*, 2001], suggest that productivity in this region was lower, in keeping with the simulation.

[44] In summary, when the combined effects of changes in dust, temperature, ice cover and circulation are included, the model reproduces roughly our reconstruction of regional changes in export production during the LGM (Figure 5). In particular, the model reproduces the latitudinal dipole in the Southern Ocean, driven in our simulations by the conjunction of dust, sea ice and circulation changes. In the N. Pacific, the limited open ocean data suggest that we correctly simulate the east-west gradient in the open ocean, but more data are needed to confirm this result.

5. Atmospheric CO$_2$ at LGM

5.1. Simulated Dust Impact

[45] When the high dust deposition rates from the LGM are used as input, our model shows an atmospheric PCO$_2$ drawdown of 15 ppm (Figure 6). Two mechanisms explain this drawdown: (1) the global increase of export production (+6%) strengthens the biological pump. Once fixed in the euphotic zone, carbon is more efficiently transferred into the deep ocean and taken away from the air-sea interface. (2) The decrease in rain ratio (−8%) increases alkalinity in sea surface waters (+8 μeq L^{-1} for the global mean), which leads to a net CO$_2$ sink. Simple calculations show that this effect accounts for more than half (−8 ppm) of the total impact.

[46] However, large uncertainties remain, in particular regarding the oceanic circulation and the sensitivity of the model to changes in high latitudes [*Archer et al.*, 2000a], the possible iron fertilization of the N-fixers in the tropical regions [*Falkowski*, 1997], and the iron cycle itself (variations in the solubility of dust, ligands and scavenging). To estimate the maximum effect of changes in dust deposition on CO$_2$ in our model, two extreme sensitivity tests were performed. The first test uses no iron deposition from the atmosphere and shows an increase of 3 ppm. This result illustrates the fact that aeolian deposition contributes only a little to the new/export production (see section 3). The second test prescribes an iron-saturated surface ocean and shows a decrease of 39 ppm, for a total extreme range of 42 ppm (Figure 6).

[47] Our best estimation (−15 ppm) for dust impact on atmospheric PCO$_2$ lies between *Archer et al.* [2000b] and *Watson et al.* [2000] estimations. In the model used by *Archer et al.* [2000b], phytoplankton speciation is not considered. Higher dust deposition rates stimulate both
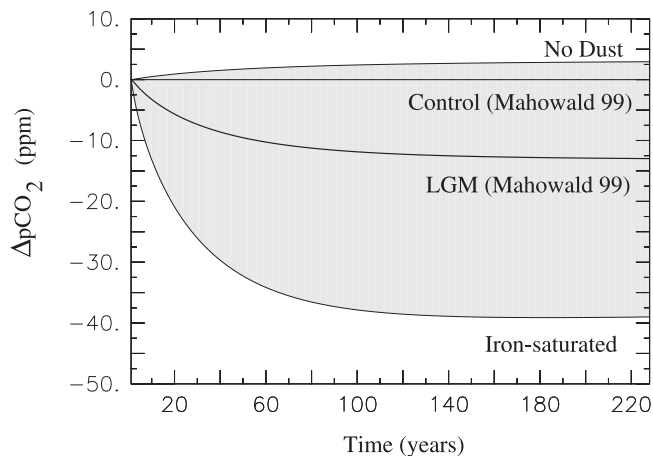

Figure 6. Dust impact on atmospheric CO$_2$ for different simulations: no atmospheric dust deposition, modern dust from *Mahowald et al.* [1999], LGM dust from *Mahowald et al.* [1999], iron-saturated ocean.

organic matter and biogenic calcite productions and do not affect the rain ratio. Their simulated impact is half as large as the one we model. *Watson et al.* [2000] model is based on a 2-D oceanic dynamical model but explicitly represents two types of phytoplankton (siliceous and nonsiliceous) in a similar way to what we have in our model. They simulate a 40 ppm drawdown in response to LGM higher deposition rates. The lower value we simulate may be explained by the fact that most of the iron utilized by phytoplankton in our model comes from the ocean's interior (by mixing with iron-rich subsurface waters) and not from atmospheric dust deposition [*Aumont et al.*, 2003]. The question of the opposition between "iron-from-below" and "iron-from-above," even in today's ocean, is still open to debate [*Aumont et al.*, 2003; *Archer and Johnson*, 2000; *Fung et al.*, 2000; *Moore et al.*, 2002]. It is a key question of the iron oceanic cycle and for its changes over glacial-interglacial periods.

[48] Also based on higher iron supply during glacial times, another mechanism has been proposed by [*Brzezinski et al.*, 2002]. Because addition of iron dramatically lowers diatom Si/N or Si/C uptake ratios [e.g., *Takeda*, 1998], *Brzezinski et al.* [2002] propose that higher iron supply during glacial times would drive the Antarctic toward N-depletion with excess silicate remaining in surface waters. They postulate that the glacial silicate-rich water may have been transported to the subtropics, favoring diatoms growth there and lowering glacial atmospheric PCO$_2$ by as much as 30–50 ppm [*Matsumoto et al.*, 2002]. In our model, we explicitly take into account the dependency of diatom Si/C uptake ratio to iron concentration [*Aumont et al.*, 2003]. However, the mechanism mentioned above has no effect on atmospheric PCO$_2$ in our simulation, certainly because we clearly underestimate Si-limitation in today's ocean [*Aumont et al.*, 2003].

5.2. Ice Cores Indications

[49] To assess the potential impact of dust on atmospheric CO$_2$ using available data, we examine Vostok records of
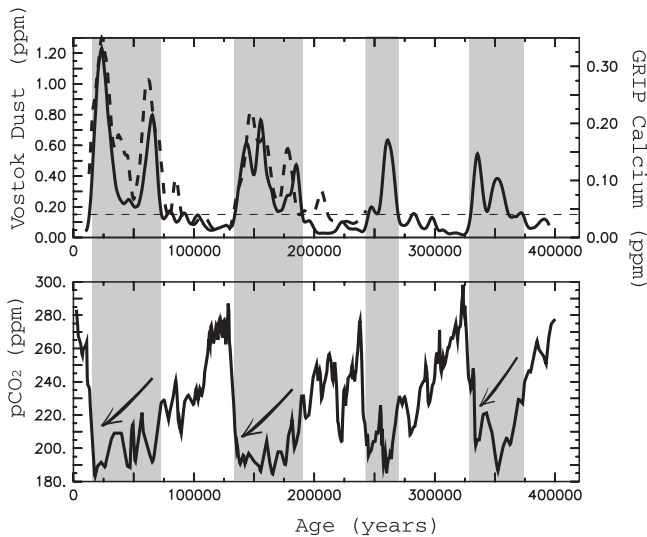
Figure 7. (top) Dust concentration from Vostok (solid line) and calcium concentration from GRIP (dashed line) [*Petit et al.*, 1999; *Fuhrer et al.*, 1993], (bottom) CO$_2$ from Vostok [*Petit et al.*, 1999]. Gray bands denote time periods when Vostok dust concentrations are above a threshold value (i.e., 0.15 ppm).

CO$_2$ and dust concentration [*Petit et al.*, 1999] and GRIP record of calcium concentration [*Fuhrer et al.*, 1993] (Figure 7).

[50] Each time when dust concentration is >0.15 ppm (gray bands on Figure 7), Vostok CO$_2$ record shows a gradual decrease from around 220 ppm to reach its full glacial value around 190 ppm. This suggests that dust deposition over the ocean may indeed affect atmospheric PCO$_2$, but with a maximum effect of about 30 ppm, consistent with the model results.

5.3. Other Effects and Uncertainties

[51] With the LGM all-effects simulation, we combine the impact of SST cooling, increase in sea-ice cover and dust deposition and circulation changes on atmospheric PCO$_2$. After more than 1000 years of simulation, the equilibrium is almost achieved and the total effect on atmospheric PCO$_2$ reaches a 30 ppm decrease.

[52] Additional simulations, taking into account each mechanism individually (dust, SSTs, sea surface salinity, sea ice and circulation) enable us to analyze each effect separately and to find the major contributors to the 30 ppm decrease.

[53] As mentioned above, LGM dust input is responsible for half of the decrease ($\sim$−15 ppm). However, a first source of uncertainty is the estimated dust reaching the ocean surface at the modern and LGM time periods, both taken from *Mahowald et al.* [1999]. As discussed in section 2.2.2, data validation suggests that this simulation matches data fairly well. However, the overall dust deposition in the Southern Hemisphere appears to be too high at the LGM. However, counterbalancing these too high deposition rates is our use of low values for the solubility of Fe in the ocean. We have used the lowest value in the range of published values (1–10%;

Fung et al. [2000]). It has recently be suggested that the solubility of Fe in dust is likely higher than 1%.

[54] Changes in circulation do not affect atmospheric PCO$_2$ significantly (see Table 3), most likely because two opposing mechanisms come into play: (1) circulations changes (vertical mixing, upwelling) affect the transport of dissolved inorganic carbon and alkalinity from the subsurface to the surface ocean, (2) but they also modify export production of organic matter and calcite from the surface ocean to intermediate and deep waters, via changes in nutrient supply (see section 3.3). For example, the decrease in the efficiency of the biological pump, driven by LGM circulation changes (the export production of organic matter decreases from 13.3 to 12 PgC y^{-1}) is counter-balanced by a reduction of vertical mixing of surface waters with subsurface DIC-rich waters.

[55] Though identified as the potential driver for the LGM low CO$_2$ level [*Stephens and Keeling*, 2000], LGM increase in sea-ice cover does not change atmospheric PCO$_2$ in our simulations. The reasons for the differences of our study from the *Stephens and Keeling* [2000] study are threefold. First, *Stephens and Keeling* [2000] prescribe an annual increase of Antarctic sea-ice cover whereas we take into account the changes in the seasonal cycle of the sea-ice cover as estimated by *Crosta et al.* [1998a]. However, an additional simulation, in which we prescribe Antarctic sea-ice cover at its winter maximum value, does not show any difference with the sea-ice seasonal-explicit simulation (Table 3). Second, oceanic circulation is very different in our oceanic general circulation model and in their box model, in particular in the Southern Ocean. Third, explicit representation of diffusion in all OGCM prevents any burying of CO$_2$ in the deep ocean as simulated by box models [*Archer et al.*, 2000a]. The fundamental behavior of box models and OGCM regarding the vertical transport of carbon was highlighted recently [*Toggweiler*, 1999; *Archer et al.*, 2000a]. The fact that changes in ice cover in our model leads to nearly no change in atmospheric CO$_2$ whereas that of *Stephens and Keeling* [2000] leads to 80 ppm is another indication that major research is needed in this field.

[56] Concerning the effect of changes in sea-surface temperatures and salinities, our results are consistent with previous studies and estimates [*Archer et al.*, 2000b; *Sigman and Boyle*, 2000]. SST cooling reduces atmospheric PCO$_2$ by 22 ppm (by 28 ppm when the tropical SST are cooled by an additional 4°C), and the estimated increase in SSS increases atmospheric PCO$_2$ by 8 ppm. In summary, our 30 ppm decrease is caused by (1) SST cooling and (2) iron fertilization of marine ecosystems.

[57] However, the simulated 30 ppm decrease is still far away from the observed 80 ppm (100–120 ppm if we take into account an LGM outgassing of 270–720 PgC [*Bird et al.*, 1994] by the land biosphere and the partial reabsorption by the ocean) and leaves more than 50 ppm to explain. Missing processes and/or systematic errors concerning aspects of our simulations may explain the discrepancy. Three main reasons have been identified. The first one concerns changes in the oceanic nitrogen budget, identified as a potential driver of LGM low atmospheric PCO$_2$ and not represented in our simulations. Increasing the glacial NO$_3^-$

inventory beyond PO$_4^{3-}$ limitation, through iron fertilization of N-fixation [*Falkowski*, 1997] or changes in denitrification rates [*Ganeshram et al.*, 2002], and assuming that the Redfield ratio of N/P of phytoplankton was higher during glacial periods, would further lead to lower atmospheric PCO$_2$. The second family of missing processes concerns changes in the alkalinity budget of the ocean [*Archer and Maier-Reimer*, 1994]. Any imbalance between CaCO$_3$ burial in the sediment and weathering on land would act to change the alkalinity budget and would impact atmospheric PCO$_2$. Third, one strong bias of our simulations is that ocean general circulation models used for simulating the ocean carbon cycle may be more diffusive than the real ocean. That would lead to underestimate the PCO$_2$ sensitivity to the biological pump as demonstrated by *Archer et al.* [2000a].

6. Conclusion

[58] We have constructed a global map of changes in export production during the LGM based on a compilation of several different paleoceanographic indicators. This map gives a strong constraint with which models can be evaluated. Our model-data comparison is encouraging, especially in the Southern Ocean and possibly also in the North Pacific, where the model qualitatively reproduces increases and decreases in export production. Nevertheless this comparison leaves room for changes in export production that are not caused by dust changes because of a lack of spatial coverage of the data. In addition, changes in magnitude are not constrained because data are essentially qualitative.

[59] Using on the one hand a compilation of paleoproductivity based on different proxies, and on the other hand phasing information between the ice core records of CO$_2$ and dust content for the last 4 glacial-interglacial cycles, we argue that the amplitude of our simulated CO$_2$ drawdown associated with high dust input is realistic and that the maximum impact of dust must be <30 ppm.

Appendix A: Fe Cycle in PISCES

[60] Here we recall the main characteristics of the parameterization of the iron cycle in PISCES. A more detailed description can be found in the work of *Aumont et al.* [2003].

[61] The approach used in PISCES is based on several assumptions. First, all the dissolved iron in seawater is supposed to be bioavailable, thus no distinction is made between the different forms of dissolved iron.

[62] Second, to account for Fe scavenging, the simple numerical model proposed by *Johnson et al.* [1997] is used. The relative constancy of deep water concentrations of Fe (around 0.6 nM) suggests that the scavenging rates of iron should strongly decrease for concentrations below the 0.6 nM limit [*Johnson et al.*, 1997]. Thus the following formulation for scavenging is used:

$$\text{Scavenging} = \lambda_{scav} \, max(0, (Fe - 0.6nM)), \qquad (A1)$$

where *Fe* is the iron concentration in nM and λ_{scav} the scavenging rate, computed as a linear function of the particle load of seawater to mimic the role of adsorption onto particles.

[63] Third, net production, exudation by phytoplankton and excretion by zooplankton affect dissolved iron concentrations through the use of an iron-to-carbon ratio (*Fe/C*). For all species except diatoms, a constant *Fe/C* is used. For diatoms, observations have shown that iron requirement for photosynthesis varies with iron availability and light level [*Sunda and Huntsman*, 1997]. Based on those considerations, an empirical relationship has been chosen to compute the *Fe/C* ratio for diatoms as a function of light and Fe concentration. Finally, the last strong assumption is that particulate organic iron is exported and remineralized at the same sinking speed and rate than particulate organic carbon.

[64] As external Fe sources, we only consider atmospheric deposition. The monthly dust deposition maps of *Mahowald et al.* [1999] (for the present and for the LGM) are used. A constant iron content of dust (3.5%), following *Fung et al.* [2000], and a constant solubility for deposited iron (1%), inside the range estimated by *Jickells and Spokes* [2001], are chosen.

References

Anderson, R., N. Kumar, R. Mortlock, P. Froelich, P. Kubik, B. Dittrich-Hannen, and M. Suter, Late Quaternary changes in productivity of the Southern Ocean, *J. Mar. Sys.*, *17*, 497–514, 1998.

Antoine, D., J. M. André, and A. Morel, Oceanic primary production, 2: Estimation at global scale from satellite (coastal zone color scanner) chlorophyll, *Global Biogeochem. Cycles*, *10*, 57–69, 1996.

Archer, D. E., and K. Johnson, A Model of the iron cycle in the ocean, *Global Biogeochem. Cycles*, *14*, 269–279, 2000.

Archer, D., and E. Maier-Reimer, Effect of deep-sea sedimentary calcite preservation on atmospheric CO$_2$ concentration, *Nature*, *367*, 260–263, 1994.

Archer, D., G. Eshel, A. Winguth, W. B. R. Pierrehumbert, M. Tobis, and R. Jacob, Atmospheric PCO$_2$ sensitivity to the biological pump in the ocean, *Global Biogeochem. Cycles*, *14*, 1219–1230, 2000a.

Archer, D., A. Winguth, D. Lea, and N. Mahowald, What caused the glacial/interglacial atmospheric pCO$_2$ cycles?, *Rev. Geophys.*, *38*, 159–189, 2000b.

Aumont, O., S. Belviso, and P. Monfray, Dimethylsulfoniopropionate (DMSP) and dimethylsulfide (DMS) sea surface distributions simulated from a global three-dimensional ocean carbon cycle model, *J. Geophys. Res.*, *107*(C4), 3029, doi:10.1029/1999JC000111, 2002.

Aumont, O., E. Maier-Reimer, S. Blain, and P. Monfray, An ecosystem model of the global ocean including Fe, Si, P co-limitations, *Global Biogeochem. Cycles*, in press, 2003.

Bacon, M. P., Glacial to interglacial changes in carbonate and clay sedimentation in the Atlantic Ocean estimated from 230 Th measurements, *Isotope Geosci.*, *2*, 97–111, 1984.

Bareille, G., M. Labracherie, P. Bertrand, L. Labeyrie, G. Lavaux, and M. Dignan, Glacial-interglacial changes in the accumulation rates of major biogenic components in Southern In-

dian Ocean sediments, *J. Mar. Sys.*, *17*, 527–539, 1998.

Barnola, J.-M., D. Raynaud, Y. Korotevich, and C. Lorius, Vostok ice core provides 160,000 year record of atmospheric CO$_2$, *Nature*, *329*, 408–414, 1987.

Behrenfeld, M., et al., Biospheric primary production during an ENSO transition, *Science*, *291*, 2594–2597, 2001.

Berger, W. H., and G. Wefer, Flux of biogenous materials to the sea floor: Open questions, in *Use and Misuse of Seafloor*, edited by K. Hsü and J. Thiede, pp. 285–304, John Wiley, New York, 1991.

Beaufort, L., Dynamics of the monsoon in the equatorial Indian Ocean over the last 260,000 years, *Quat. Int.*, *31*, 13–18, 2000.

Bird, M. I., J. Lloyd, and G. Farquhar, Terrestrial carbon storage at the LGM, *Nature*, *371*, 566, 1994.

Blanke, B., and P. Delecluse, Low frequency variability of the tropical Atlantic ocean simulated by a general circulation model with mixed layer physics, *J. Phys. Oceanogr.*, *23*, 1363–1388, 1993.

Bonn, W. J., F. X. Gingele, H. Grobe, A. Mackensen, and D. K. Futterer, Paleoproductivity at the Antarctic continental margin: Opal and barium records for the last 400 ka, *Palaeogeogr. Palaeoclimatol. Palaeoecol.*, *139*, 195–211, 1998.

Boyd, P., et al., A mesoscale phytoplankton bloom in the polar Southern Ocean stimulated by iron fertilization, *Nature*, *407*, 695–702, 2000.

Boyle, E., Chemical accumulation variations under the Peru Current during the Past 130,000 years, *J. Geophys. Res.*, *88*, 7667–7680, 1983.

Broecker, W. S., Glacial to interglacial changes in ocean chemistry, *Prog. Oceanogr.*, *11*, 151–197, 1982.

Brzezinski, M. A., C. J. Pride, V. M. Franck, D. M. Sigman, J. L. Sarmiento, K. Matsumoto, N. Gruber, G. H. Rau, and K. H. Coale, A switch from Si(OH)$_4$ to NO$_3^-$ depletion in the glacial Southern Ocean, *Geophys. Res. Lett.*, *29*(12), 1564, doi:10.1029/2001GL014349, 2002.

Ceccaroni, L., M. Frank, M. Frignani, L. Langone, M. Ravaioli, and A. Mangini, Late Quaternary fluctuations of biogenic component fluxes on the continental slope of the Ross Sea and Antarctica, *J. Mar. Sys.*, *17*, 515–525, 1998.

Chase, Z., R. Anderson, M. Fleisher, and P. Kubik, Accumulation of biogenic and lithogenic material in the Pacific sector of the Southern Ocean during the past 40,000 years, *Deep Sea Res., Part II*, *50*(3–4), 799–832, 2003.

Claquin, T., et al., Radiative forcing of climate by ice-age dust, *Clim. Dyn.*, *20*, 193–202, 2003.

CLIMAP, Seasonal reconstruction of the earth's surface at the last glacial maximum, *Tech. Rep. Map and Chart Ser. MC 36*, Geol. Soc. of Am., Boulder, Colo., 1981.

Coale, K., et al., A massive phytoplankton bloom induced by an ecosystem-scale iron fertilization experiment in the equatorial Pacific Ocean, *Nature*, *383*, 495–501, 1996.

Crosta, X., J.-J. Pichon, and L. Burckle, Reappraisal of Antarctic seasonal sea-ice at the Last Glacial Maximum, *Geophys. Res. Lett.*, *25*, 2703–2706, 1998a.

Crosta, X., J.-J. Pichon, and L. Burckle, Application of modern analog technique to marine Antarctic diatoms: Reconstruction of maximum sea-ice extent at the Last Glacial Maximum, *Paleoceanography*, *13*, 284–297, 1998b.

Duplessy, J.-C., L. D. Labeyrie, A. Juillet-Leclerc, F. Maitre, J. Duprat, and M. Sarnthein, Surface salinity reconstruction of the North Atlantic ocean during the last glacial maximum, *Oceanogr. Acta*, *14*, 311–323, 1991.

Esbensen, S. K., and Y. Kushnir, The heat budget of the global ocean: An atlas based on estimates from marine surface observations, *Tech. Rep. 29*, Clim. Resolut. Inst., Oreg. State Univ., Corvallis, Oreg., 1981.

Falkowski, P. G., Evolution of the nitrogen cycle and its influence on the biological sequestration of CO$_2$ in the ocean, *Nature*, *387*, 272–275, 1997.

Francois, R., P. Bacon, M. Altabet, and L. Labeyrie, Glacial/interglacial changes in sediment rain rate in the SW Indian sector of subantarctic waters as recorded by 230 Th and 231 Pa and U and d15N, *Paleoceanography*, *8*, 611–629, 1993.

Frank, M., R. Gersonde, M. R. van der Loeff, G. Bohrmann, C. C. Nrnberg, M. Suter, and A. Mangini, Similar glacial and interglacial export bioproductivity in the Atlantic sector of the Southern Ocean: Multiproxy evidence and implications for glacial atmospheric CO$_2$, *Paleoceanography*, *15*, 642–658, 2000.

Fuhrer, K., A. Neftel, M. Anklin, and V. Maggi, Continuous measurements of hydrogen peroxide, formaldehyde, calcium and ammonium concentrations along the new GRIP ice core from Summit, central Greenland, *Atmos. Environ.*, *12*, 1873–1880, 1993.

Fung, I. Y., S. K. Meyn, I. Tegen, S. C. Doney, J. John, and J. Bishop, Iron supply and demand in the upper ocean, *Global Biogeochem. Cycles*, *14*, 281–295, 2000.

Ganeshram, R., and T. Pedersen, Glacial-interglacial variability in upwelling and bioproductivity off NW Mexico: Implications for Quaternary paleoclimate, *Paleoceanography*, *13*, 634–645, 1998.

Ganeshram, R., T. Pedersen, S. Calvert, and R. Francois, Reduced nitrogen fixation in the glacial ocean inferred from changes in marine nitrogen and phosphorus inventories, *Nature*, *415*, 156–159, 2002.

Hebbeln, D., M. Marchant, and G. Wefer, Paleoproductivity in the southern Peru-Chile Current through the last 33,000 years, *Mar. Geol.*, in press, 2002.

Hellermann, S., and M. Rosenstein, Normal monthly windstress over the world ocean with error estimates, *J. Phys. Oceanogr.*, *24*, 619–637, 1983.

Herbert, T., et al., Collapse of the California Current during glacial maxima linked to climate change on land, *Science*, *293*, 71–76, 2001.

Herguera, J., Deep-sea benthic foraminifera and biogenic opal—Glacial to postglacial productivity changes in the western equatorial Pacific, *Mar. Micropaleontol.*, *19*, 79–98, 1992.

Herguera, J., Last glacial paleoproductivity patterns in the eastern equatorial Pacific: Benthic foraminifera records, *Mar. Micropaleontol.*, *40*, 259–275, 2000.

Hinrichs, K.-U., R. Schneider, P. Mller, and J. Rullktter, A biomarker perspective on paleoproductivity variations in two late Quaternary sediment sections from the southeast Atlantic Ocean, *Org. Geochem.*, *30*, 341–366, 1999.

Huang, C.-Y., P.-M. Liew, M. Zhao, T.-C. Chang, C.-M. Kuo, M.-T. Chen, C.-H. Wang, and L.-F. Zheng, Deep sea and lake records of the southeast Asian paleomonsoons for the last 25 thousand years, *Earth Planet. Sci. Lett.*, *146*, 59–72, 1997.

Ikehara, M., K. Kawamura, N. Ohkouchi, M. Murayama, T. Nakamura, and A. Taira, Variations of terrestrial input and marine productivity in the Southern Ocean (48S) during the last two deglaciations, *Paleoceanography*, *15*, 170–180, 2000.

Jahnke, R. A., The global ocean flux of particulate organic carbon: Areal distribution and magnitude, *Global Biogeochem. Cycles*, *10*, 71–88, 1996.

Jickells, T. D., and L. J. Spokes, Atmospheric iron inputs to the oceans, in *Biogeochemistry of Iron in Seawater*, SCOR/UIUPAC Ser., edited by D. R. Turner and K. Hunter, pp. 85–121, John Wiley, New York, 2001.

Johnson, K. S., R. M. Gordon, and K. H. Coale, What controls dissolved iron in the world ocean?, *Mar. Chem.*, *57*, 137–161, 1997.

Jorissen, F. J., D. Barmawidjaja, S. Puskaric, and G. van der Zwaan, Vertical distribution of benthic foraminifera in the northern Adriatic Sea: The relation with the organic flux, *Mar. Micropaleontol.*, *19*, 131–146, 1992.

Kasten, S., R. Haese, M. Zabel, C. Rhlemann, and H. Schulz, Barium peaks at glacial terminations in sediments of the equatorial Atlantic Ocean—Relics of deglacial productivity pulses?, *Chem. Geol.*, *175*, 635–651, 2001.

Kawahata, H., Fluctuations in the ocean environment within the western Pacific warm pool during late Pleistocene, *Paleoceanography*, *14*, 639–652, 1999.

Kawahata, H., Shifts in oceanic and atmospheric boundaries in the Tasman Sea (southwest Pacific) during the Late Pleistocene: Evidence from organic carbon and lithogenic fluxes, *Palaeogeogr. Palaeoclimatol. Palaeoecol.*, *184*, 225–249, 2002.

Kawahata, H., and N. Eguchi, Iogenic sediments on the Eauripik Rise of the western equatorial Pacific during the late Pleistocene, *Geochem. J.*, *30*, 201–215, 1996.

Kawahata, H., A. Suzuki, and N. Ahagon, Biogenic sediments in the west Caroline Basin and the western equatorial Pacific during the last 330,000 years, *Mar. Geol.*, *149*, 155–176, 1998.

Kawahata, H., K. I. Ohkushi, and Y. Hatakeyama, Comparative Late Pleistocene paleoceanographic changes in the midlatitude boreal and austral western Pacific, *J. Oceanogr.*, *55*, 747–761, 1999.

Kawahata, H., T. Okamoto, E. Matsumoto, and H. Ujiie, Fluctuations of eolian flux and ocean productivity in the mid-latitude North Pacific during the last 200 kyr, *Quat. Sci. Rev.*, *9*, 1279–1282, 2000.

Keigwin, L., Glacial-age hydrography for the far northwest Pacific Ocean, *Paleoceanography*, *13*, 323–339, 1998.

Kirst, G., R. Schneider, P. Mller, I. von Storch, and G. Wefer, The Late Quaternary Benguela Current system: Implications from alkenone-derived sea surface temperature and organic carbon records, *Quat. Res.*, *52*, 92–103, 1999.

Klump, J., D. Hebbeln, and G. Wefer, The impact of sediment provenance on barium-based productivity estimates, *Mar. Geol.*, *169*, 259–271, 2000.

Knox, F., and M. McElroy, Changes in atmospheric CO$_2$: Influence of marine biota at high latitudes, *J. Geophys. Res.*, *89*, 4629–4637, 1984.

Kohfeld, K. E., and S. P. Harrison, Records of aeolian dust deposition on the Chinese Loess Plateau during the late Quaternary, *Quat. Sci. Rev.*, in press, 2003.

Koopmann, B., Sedimentation von Saharastaub im subtropischen Nordatlantik whrend der letzten 25.000 Jahre, *Meteorol. Forsch. Ergebnisse*, 35, 23–59, 1981.

Koschmeider, C., Zeitlich hochaurlsende Rekonstruktion von sptquartren Sedimentationsbedingungen im Sdatlantik mit Hilfe von 230Th, MS thesis, Univ. Heidelberg, Heidelberg, 1996.

Kumar, N., R. F. Anderson, R. A. Mortlock, P. N. Froelich, P. Kubik, A. Dittrich-Hannen, and M. Suter, Increased biological productivity and export production in the glacial Southern Ocean, *Nature*, 378, 675–680, 1995.

Laws, E. A., P. G. Falkowski, W. O. Smith Jr., H. Ducklow, and J. J. McCarthy, Temperature effects on export production in the open ocean, *Global Biogeochem. Cycles*, 14(4), 1231–1246, 2000.

Loubere, P., A multiproxy reconstruction of biological productivity and oceanography in the eastern equatorial Pacific for the past 30,000 years, *Mar. Micropaleontol.*, 37, 173–198, 1999.

Lyle, M., D. Murray, B. Finney, J. Dymond, J. Robbins, and K. Brookforce, The record of Late Pleistocene biogenic sedimentation in the eastern tropical Pacific Ocean, *Paleoceanography*, 3, 39–59, 1988.

Madec, G., P. Delecluse, M. Imbard, and C. Lévy, OPA Version 8.0 Ocean General Circulation model, *Reference Manual*, Lab. d'Oceanogr. Dyn. et de Climatol., Paris, 1997.

Mahowald, N., K. K. M. Hansson, Y. Balkanski, S. P. Harrison, I. C. Prentice, M. Schulz, and H. Rodhe, Dust sources and deposition during the last glacial maximum and current climate: A comparison of model results with paleodata from ice cores and marine sediments, *J. Geophys. Res.*, 104, 15,895–15,916, 1999.

Manighetti, B., and I. McCave, Depositional fluxes and palaeoproductivity and ice rafting in the NE Atlantic over the past 30 ka, *Paleoceanography*, 10, 579–592, 1995.

Marcantonio, F., R. Anderson, S. Higgins, M. Fleisher, M. Stute, and P. Schlosser, Abrupt intensification of the SW Indian Ocean monsoon during the last deglaciation: Constraints from Th and Pa and He isotopes, *Earth Planet. Sci. Lett.*, 184, 505–514, 2001a.

Marcantonio, F., R. Anderson, S. Higgins, M. Stute, and P. Schlosser, Sediment focusing in the central equatorial Pacific Ocean, *Paleoceanography*, 16, 260–267, 2001b.

Martin, J. H., Glacial-interglacial CO$_2$ changes: The iron hypothesis, *Paleoceanography*, 5, 1–13, 1990.

Martin, J. H., and S. E. Fitzwater, Iron deficiency limits phytoplankton growth in the northeast Pacific subarctic, *Nature*, 331, 341–343, 1988.

Martinez, P., et al., An integrated view of inorganic and organic biogeochemical indicators of paleoproductivity changes in a coastal upwelling area, *Org. Geochem.*, 24, 411–420, 1996.

Matsumoto, K., J. L. Sarmiento, and M. A. Brzezinski, Silicic acid leakage from the Southern Ocean: A possible explanation for glacial atmospheric *p*CO$_2$, *Global Biogeochem. Cycles*, 16(3), 1031, doi:10.1029/2001GB001442, 2002.

McDonald, D., T. Pedersen, and J. Crusius, Multiple late Quaternary episodes of exceptional diatom production in the Gulf of Alaska, *Deep Sea Res. Part II*, 46, 2993–3017, 1999.

McManus, J., et al., Geochemistry of barium in marine sediments: Implications for its use as a paleoproxy, *Geochim. Cosmochim. Acta*, 62, 2453–2473, 1998.

Mix, A. C., N. G. Pisias, and S. W. Hostetler, Foraminiferal faunal estimates of paleotemperature: Circumventing the no-analog problem yields cool ice age tropics, *Paleoceanography*, 14, 350–359, 1999.

Moore, J. K., S. C. Doney, D. M. Glover, and I. Y. Fung, Iron cycling and nutrient limitation patterns in surface waters of the world ocean, *Deep Sea Res. Part II*, 49, 463–507, 2002.

Moreno, A., S. Nave, H. Kuhlmann, M. Canals, J. Targarona, T. Freudenthal, and F. Abrantes, Productivity response in the North Canary Basin to climate changes during the last 250,000 yr: A multi-proxy approach, *Earth Planet. Sci. Lett.*, 196, 147–159, 2002.

Mueller, A., and B. Opdyke, Glacial-interglacial changes in nutrient utilization and paleoproductivity in the Indonesian Throughflow, *Paleoceanography*, 15, 85–94, 2000.

Mueller, P., R. Schneider, and G. Ruhland, Late Quaternary PCO$_2$ variations in the Angola Current: Evidence from organic carbon d13C and alkenone temperatures, in *Carbon Cycling in the Glacial Ocean: Constraints on the Ocean's Role in Global Change*, edited by R. Zhang et al., pp. 343–366, Springer-Verlag, New York, 1994.

Okhouchi, N., K. Kawamura, and A. Taira, Fluctuations of terrestrial and marine biomarkers in the western tropical Pacific during the last 23,300 years, *Paleoceanography*, 12, 623–630, 1997.

Paytan, A., M. Kastner, and F. Chavez, Glacial to interglacial fluctuations in productivity in the equatorial Pacific as indicated by marine barite, *Science*, 274, 1355–1357, 1996.

Pedersen, T., Increased productivity in the eastern equatorial Pacific during the Last Glacial Maximum (19,000 to 14,000 yr BP), *Geology*, 11, 16–19, 1983.

Pedersen, T., M. Pickering, J. Vogel, J. Southon, and D. Nelson, The response of benthic foraminifera to productivity cycles in the eastern equatorial Pacific: Faunal and geochemical constraints on glacial bottom water oxygen levels, *Paleoceanography*, 3, 157–168, 1988.

Pedersen, T., B. Nielsen, and M. Pickering, Timing of late Quaternary productivity pulses in the Panama basin and implications for atmospheric CO$_2$, *Paleoceanography*, 6, 657–677, 1991.

Petit, J. R., et al., Climate and atmospheric history of the past 420,000 years from the Vostok ice, Antarctica, *Nature*, 399, 429–436, 1999.

Pichon, J., L. Labeyrie, G. Bareille, M. Labracherie, J. Duprat, and J. Jouzel, Surface water temperature changes in the high latitudes of the Southern Hemisphere over the last glacial-interglacial cycle, *Paleoceanography*, 7, 289–318, 1992.

Pinot, S., G. Ramstein, I. Marsiat, A. de Vernal, O. Peyron, J.-C. Duplessy, and M. Weinelt, Sensitivity of the European LGM climate to North Atlantic sea-surface temperature, *J. Geophys. Res.*, 26, 1893–1896, 1999.

Rea, D., The paleoclimatic record provided by eolian deposition in the deep sea: The geologic history of wind, *Rev. Geophys.*, 32, 159–195, 1994.

Rea, D., N. Pisias, and T. Newberry, Late Pleistocene paleoclimatology of the central equatorial Pacific: Flux patterns of biogenic sediments, *Paleoceanography*, 6, 227–244, 1991.

Ruddiman, W., Tropical Atlantic terrigenous fluxes since 25,000 yrs BP, *Mar. Geol.*, 136, 189–207, 1997.

Ruhlemann, M., M. Frank, W. Hale, A. Mangini, S. Mulitza, P. Mller, and G. Wefer, Late Quaternary productivity changes in the western equatorial Atlantic: Evidence from 230 Th-normalized carbonate and organic carbon accumulation rates, *Mar. Geol.*, 135, 127–152, 1996.

Rutsch, H.-J., A. Mangini, G. Bonani, B. Dittrich-Hannen, P. Kubik, M. Suter, and M. Segl, 10 Be and Ba concentrations in west African sediments trace productivity in the past, *Earth Planet. Sci. Lett.*, 133, 129–143, 1995.

Sarmiento, J. L., and J. R. Toggweiler, A new model for the role of the oceans in determining atmospheric PCO$_2$, *Nature*, 308, 621–624, 1984.

Sarmiento, J. L., J. Dunne, A. Gnanadesikan, R. M. Key, K. Matsumoto, and R. Slater, A new estimate of the CaCO$_3$ to organic carbon export ratio, *Global Biogeochem. Cycles*, 16(4), 1107, doi:10.1029/2002GB001919, 2002.

Schlitzer, R., Carbon export fluxes in the Southern Ocean: results from inverse modeling and comparison with satellite-based estimates, *Deep Sea Res. Part II*, 49, 1623–1644, 2002.

Schmiedl, G., and A. Mackensen, Late Quaternary paleoproductivity and deep water circulation in the eastern South Atlantic Ocean: Evidence from benthic foraminifera, *Palaeogeogr. Palaeoclimatol. Palaoecol.*, 130, 43–80, 1997.

Schneider, R., P. Mueller, and G. Ruhland, Late Quaternary surface circulation in the east-equatorial South Atlantic: Evidence from alkenone sea surface temperatures, *Paleoceanography*, 10, 197–219, 1995.

Schneider, R., B. Price, P. Mller, D. Kroon, and I. Alexander, Monsoon related variations in Zaire (Congo) sediment load and influence of fluvial silicate supply on marine productivity in the east equatorial Atlantic during the last 200,000 years, *Paleoceanography*, 12, 463–481, 1997.

Seki, O., K. Kawamura, T. Nakatsuka, K. Ohnishi, M. Ikehara, and M. Wakatsuchi, Sediment core profiles of long-chain n-alkanes in the Sea of Okhotsk: Enhanced transport of terrestrial organic matter from the last deglaciation to the early Holocene, *Geophys. Res. Lett.*, 30(1), 1001, doi:10.1029/2001GL014464, 2003.

Shackleton, N. J., Carbon-13 in Uvigerina: Tropical rainforest history and the equatorial Pacific carbonate dissolution cycles, in *The Fate of Fossil Fuel CO$_2$ in the Oceans*, edited by N. R. Andersen and A. Malahoff, pp. 401–428, Plenum, New York, 1977.

Sicre, M.-A., Y. Ternois, M. Paterne, A. Boireau, L. Beaufort, P. Martinez, and P. Bertrand, Biomarker stratigraphic records over the last 150 kyr off the NW African coast at 25 deg N, *Org. Geochem.*, 31, 577–588, 2000.

Siegenthaler, U., and T. Wenk, Rapid atmospheric CO$_2$ variations and ocean circulation, *Nature*, 308, 624–625, 1984.

Sigman, D., and E. A. Boyle, Glacial/interglacial variations in atmospheric carbon dioxide, *Nature*, 407, 859–869, 2000.

Six, K. D., and E. Maier-Reimer, Effects of plankton dynamics on seasonal carbon fluxes in an ocean general circulation model, *Global Biogeochem. Cycles*, 10, 559–583, 1996.

Sonzogni, C., E. Bard, and F. Roster, Tropical sea-surface temperatures during the last glacial period: A view based on alkenones in Indian Ocean sediments, *Quat. Sci. Rev.*, 17, 1185–1201, 1998.

Stephens, B. B., and R. F. Keeling, The influence of Antarctic sea ice on glacial-intergalcial CO₂ variations, *Nature*, *404*, 171–175, 2000.

Stephens, M., and D. Kadko, Glacial-Holocene calcium carbonate dissolution at the central equatorial Pacific seafloor, *Paleoceanography*, *12*, 797–804, 1997.

Sunda, W. G., and S. A. Huntsman, Interrelated influence of iron, light and cell size on marine phytoplankton growth, *Nature*, *390*, 389–392, 1997.

Takeda, S., Influence of iron availability on nutrient consumption ratio of diatoms in oceanic waters, *Nature*, *393*, 774–777, 1998.

Ternois, Y., M.-A. Sicre, and M. Paterne, Climatic changes along the northwestern African continental margin over the last 30 kyrs, *Geophys. Res. Lett.*, *27*, 133–136, 2000.

Ternois, Y., K. Kawamura, L. Keigwin, N. Ohkouchi, and T. Nakatsuka, A biomarker approach for assessing marine and terrigenous inputs to the sediments of Sea of Okhotsk for the last 27,000 years, *Geochim. Cosmochim. Acta*, *65*, 791–802, 2001.

Thompson, L., Ice core evidence for climate change in the Tropics: Implications for our future, *Quat. Sci. Rev.*, *19*, 19–35, 2000.

Toggweiler, J. R., Variations of atmospheric CO₂ driven by ventilation of the ocean's deepest water, *Paleoceanography*, *14*, 571–588, 1999.

Villanueva, J., J. Grimalt, E. Cortijo, L. Vidal, and L. Labeyrie, A biomarker approach to the organic matter deposited in the North Atlantic during the last climatic cycle, *Geochim. Cosmochim. Acta*, *61*, 4633–4646, 1997.

Watson, A. J., D. C. E. Bakker, A. J. Ridgwell, P. W. Boyd, and C. S. Law, Effect of iron supply on Southern Ocean CO₂ uptake and implications for glacial atmospheric CO₂, *Nature*, *407*, 730–733, 2000.

Weaver, A. J., M. Eby, F. F. Augustus, and E. C. Wiebe, Simulated influence of carbon dioxide, orbital forcing and ice-sheets on the climate of the Last Glacial Maximum, *Nature*, *394*, 847–853, 1998.

Wefer, G., P. Heinze, and E. Suess, Stratigraphy and sedimentation rates from oxygen isotope composition and organic carbon content and grain-size distribution at the Peru upwelling region: Holes 680B and 686B, *Proc. Ocean Drill. Prog. Sci. Results*, *112*, 355–367, 1990.

Wollenburg, J., W. Kuhnt, and A. Mackensen, Changes in Arctic Ocean paleoproductivity and hydrography during the last 145 kyr: The benthic foraminiferal record, *Paleoceanography*, *16*, 65–77, 2001.

Yamanaka, Y., and E. Tajika, The role of the vertical fluxes of particulate organic matter and calcite in the oceanic carbon cycle: Studies using an ocean biogeochemical general circulation model, *Global Biogeochem. Cycles*, *10*, 361–382, 1996.

————————————

O. Aumont, Laboratoire d'Océanographie et de Dynamique du Climat, Université Paris VI, Place Jussieu, F-75005 Paris Cedex, France. (aumont@lodyc.jussieu.fr)

L. Bopp, Laboratoire des Sciences du Climat et de l'Environnement, CE-Saclay, Orme des Merisiers, F-91191 Gif sur Yvette, France. (bopp@lsce.saclay.cea.fr)

K. E. Kohfeld and C. Le Quéré, Max-Planck Institut für Biogeochemie, Postfach 100164, D-07701 Jena, Germany. (kek@bgc-jena.mpg.de; lequere@bgc-jena.mpg.de)
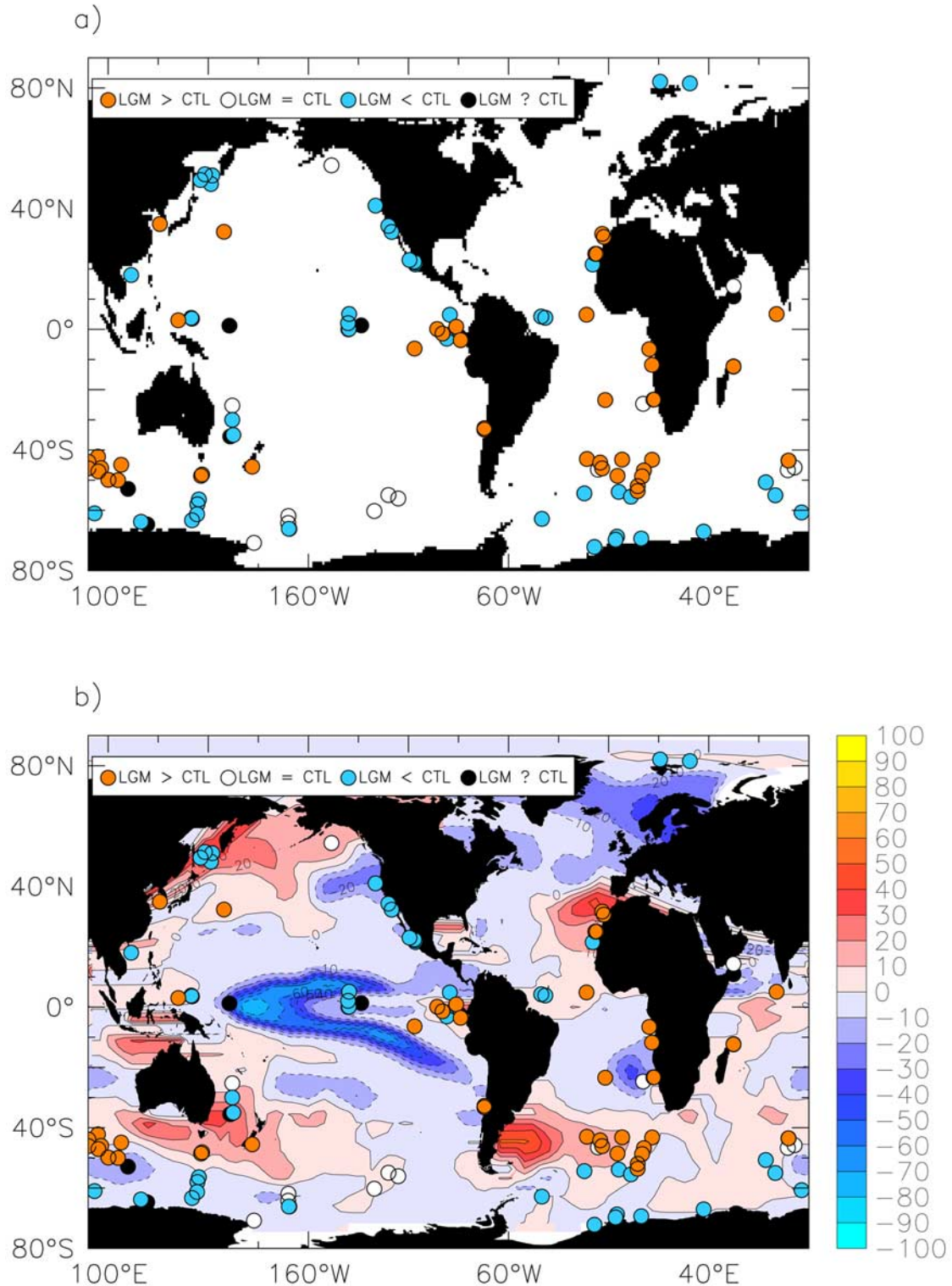
Figure 5. Export production (EP) for the LGM minus today. (a) The top panel shows whether the EP increased (LGM > CTL), decreased (LGM < CTL), remained the same (LGM = CTL) or is undetermined (LGM ? CTL) during the LGM compared to today (CTL for control). This information is based on our analysis of various paleodata indicators (complete references of the data sources is given in Table 1). (b) The bottom panel shows a comparison of simulated changes in export production (gC/m^2/y) with the paleoceanographic data. The simulated changes combine effects of LGM dust [*Mahowald et al.*, 1999], Antarctic sea ice [*Crosta et al.*, 1998a], SSTs [*CLIMAP*, 1981], and circulation changes.